Chapter 4

Morphologically modified MOP-Am2 as a Reusable Facilitator for Acceptorless Dehydrogenative Annulation of Alcohols

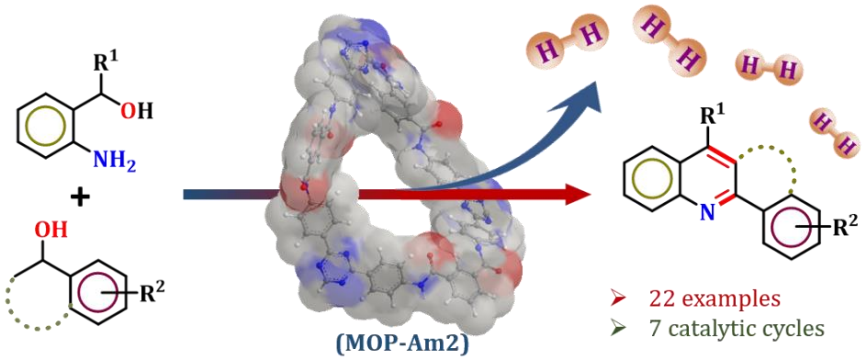

4.1 Introduction

The quinoline scaffold is found in a wide range of natural chemicals and pharmacologically active drugs, accounting for a sizable portion of the pharmaceutical industry [1,2]. The traditional methods for synthesizing this heterocyclic skeleton need the use of costly starting materials and high temperatures [3,4]. Most of the quinoline derivatives are known for their *anti*-malarial, anticancer, *anti*-Alzheimer's, *anti*-HIV, and agrochemical activities and also known for OLED applications in material chemistry [5-10]. Few of the biologically active molecules having quinoline moieties are exemplified below (Figure 4.1).

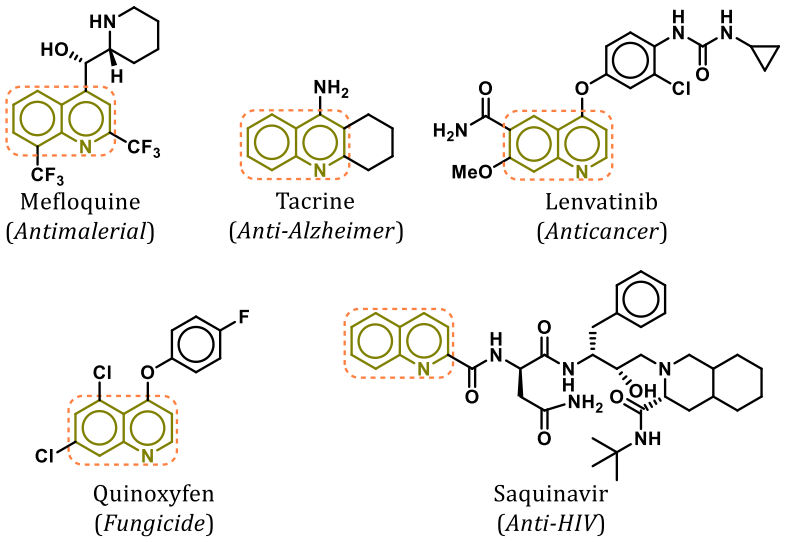

Figure 4.1 Examples of bioactive molecules containing quinoline scaffold

The development of several synthetic techniques for effective quinoline synthesis have been sparked by the significance of quinoline scaffolds to date. Commonly known methodologies for quinoline synthesis include Skraup, Pfitzinger, Doebner-von Miller, Conrad-Limpach, and Friedländer annulation [3]. Among them Friedländer annulation is considered as the direct classical path for quinoline synthesis since long with lots of limitations such as harsh reaction condition, low stability of the reactants, and multiple steps corresponding to a lower productivity [11]. Later, reports suggested transition metal driven system for modified Friedländer quinoline synthesis that included metal complexes of Pd, Ru, Ir or Rh etc [12,13]. Other reported abundant metal complexes contain Cu, Fe, Ni, Mn, Cu, Co etc, ignoring concerns of metal toxicity, stoichiometric catalyst loading and reusability

[14,18]. But an environmentally benign, sustainable, metal and oxidant free system with an affordable efficiency is yet a challenge.

A. Friedländer annulation for quinoline synthesis [11].

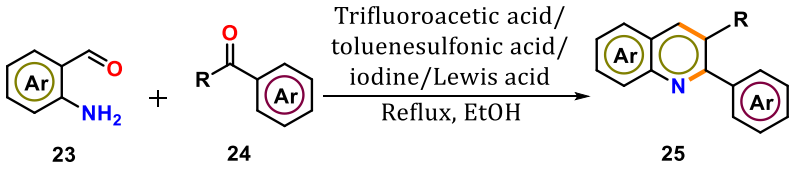

23 24 25

B. Pd catalysed intermolecular aerobic annulation for quinoline synthesis [12].

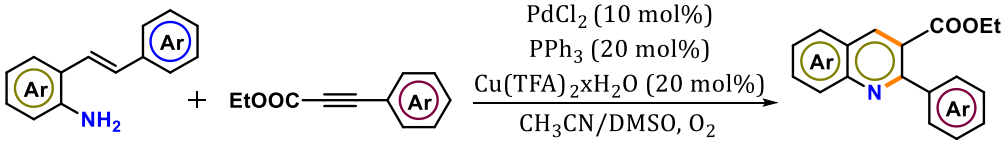

26 27 28

In search of the greener approach for the synthesis of quinoline, Wan and co-worker introduced ethyl lactate as a mediator third component for such synthesis from aldehyde and aniline catalysed by $FeCl_3$ [19]. However, stoichiometric use of highly reactive aldehyde brings drawbacks for such transformation reaction because of the low stability and easily air oxidized substrates.

In recent years, dehydrogenation of alcohols has evolved as a unique advantageous prototype to synthesize heterocycle by enabling oxidative transformation without relying on an external oxidant [20-21]. Common strategy usually demands expensive metal complex and/or ions [17,22-24]. Recent breakthrough by Xu and coworkers demonstrated a metal free protocol where anthraquinone as an organic small-molecule catalyst and DMSO as an oxidant for quinoline synthesis from 2-aminobenzyl alcohol driven by visible light [25].

C. Fe catalysed ethyl lactate based quinoline synthesis [19].

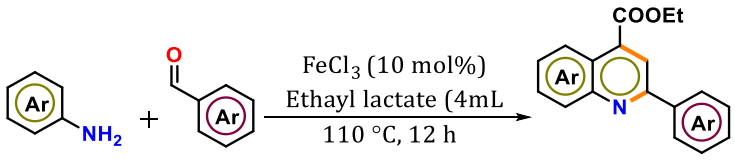

29 30 31

D. Visible light driven quinoline synthesis [25].

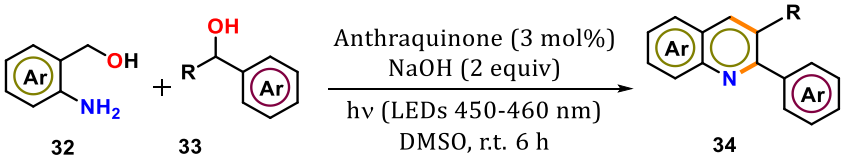

32 33 34

The dehydrogenation of alcohols over porous organic polymers (POPs) has already been well-established in Chapter 2 [26,27]. The ability to leverage such important reactions towards various organic transformations depends upon the molecular architecture of the extended polymers. This inspired us to think of metal free POPs as a sustainable and benign organocatalyst for the synthesis of valued quinoline scaffolds from alcohols *via in-situ* generation of H_2. The evolutionary one pot multistep synthetic route over classical methods, for medicinally and industrially valued quinoline derivatives offers a great strategy to avoid the use of unstable reactants, harsh reaction conditions, and low productivity.

Improvising the catalytic activity and assimilating the benefits of heteroatom, our prime interest lies in employing triazine MOP-Am2 that might show great efficiency towards oxidative cyclization reaction or annulation of alcohols to quinoline (Scheme 4.1). Alongside synthetic modification was performed on MOP-Am2 to enhance the catalytic efficiency of the organocatalyst by changing the morphology. The morphological modification or variance and better surface area obtained during nucleation growth of the polymer compared to the previous reports in Chapter 2 & 3 was evidenced as a remarkable and reusable catalyst for fabricating oxidative annulation of alcohols to quinoline. Unlike the other metal free catalysts, MOP-Am2 denies the use of any external oxidant. Indeed, the electron rich surface of MOP-Am2 drives the reaction by oxidizing the alcohol under basic media at moderate temperature.

This work

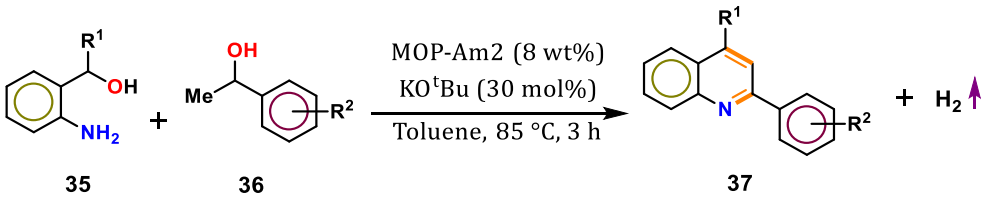

Scheme 4.1 Oxidative annulations of 1° and 2° alcohols to corresponding quinolone derivatives

This protocol features incomparable advantages of greener approach such as (i) avoid metal toxicity, (ii) oxidant-free oxidation, (iii) H_2 evolution and H_2O as by-product, and (iv) excellent catalyst recovery.

4.2 Results and Discussion

4.2.1 Synthesis of morphology modified MOP-Am2

In order to construct the morphology modified MOP-Am2, similar protocol has been followed as Scheme 2.2 in chapter 2. After filtration the so obtained pale yellow solid was refluxed with acetonitrile for another 24 h (Scheme 4.2). The precipitate was then filtered, washed several times with acetone and dried under vacuum at 100 °C for 24 h; characterized with the requisite analysis.

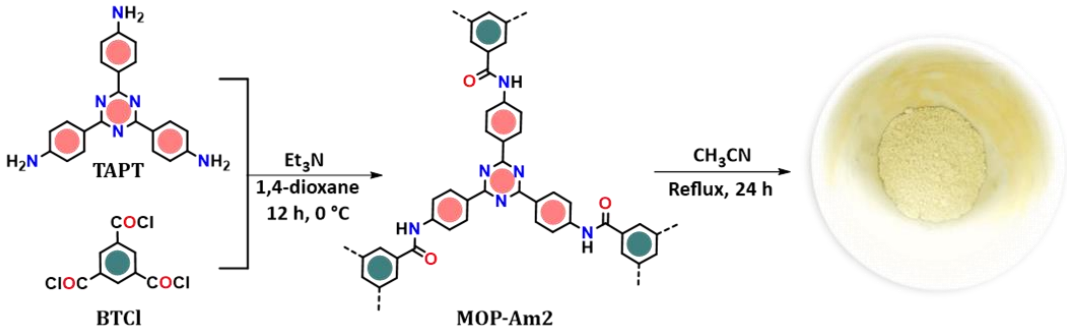

Scheme 4.2 Synthesis of morphologically modified MOP-Am2

Once the similar structural integrity as in Scheme 2.2 was established by FT-IR, solid-state ^{13}C CP/MAS NMR, PXRD and EDX analysis, we sought to proceed for morphological investigation with FESEM and TEM analyses.

FESEM analysis on modified MOP-Am2 revealed a globular morphology with rough surface (Figure 4.1a) instead of spider web-like structure reported earlier (Chapter 2, Figure 2.3a).

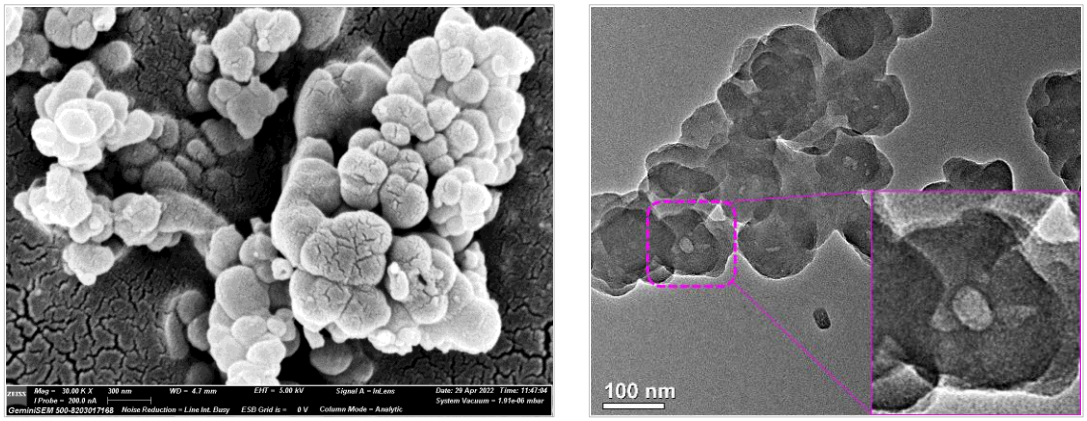

(a) (b)

Figure 4.2 (a) FESEM analysis suggested the globular rough surface and (b) TEM analysis suggested a hollow-spherical morphology of the material

The thermal treatment on the MOP-Am2 with acetonitrile nucleates the particle in globular morphology. Besides the TEM analysis also verified the effect of thermal treatment on nucleation behaviour of MOP-Am2. Figure 4.1b showed a TEM of hollow-spherical morphology of the material instead of sheet like structures established previously (Chapter 2, Figure 2.3b).

This observed morphological behaviour is due to Oswald ripening [28,29]. The polymeric formation of MOP-Am2 occurred even at low temperature due to high reactivity of BTCl [26]. However, refluxing it with acetonitrile at high temperature, the smaller particles at the inner portion of the sheet like structures of MOP-Am2 started decomposing into individual crystallites. These crystallites then started nucleating along the periphery of MOP-Am2 due to surface energy minimization eventually causing hollow-spherical aggregation.

The effect of thermal treatment was also observed on the surface area of MOP-Am2. The BET analysis with N_2 at 77 K anticipated a typical type IV reversible sorption isotherm (Figure 4.3) with a better surface area of 92 m^2g^{-1} than that obtained from the previously reported method of preparation (Chapter 2, Figure 2.2d). This might arise because of the morphological variation in the MOP-Am2 with lower surface energy which increases the overall reactive sites. The pore size distribution plot in Figure 4.3 (inset) displayed a narrow pore width distribution at 1.5 nm diameter which conferred the modified MOP-Am2 still a microporous in nature.

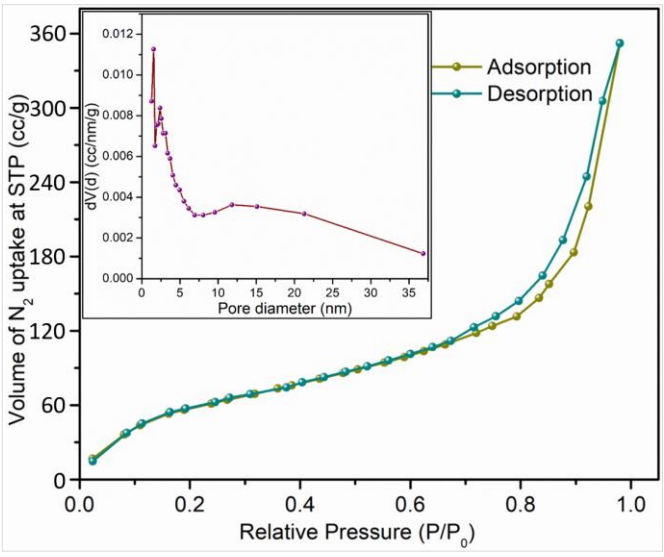

Figure 4.3 BET sorption plot of N_2 at 77 K demonstrates the type IV isotherm. The pore size distribution plot (inset) determined MOP-Am2 to be microporous in nature

To determine the catalytic potency of morphology modified MOP-Am2, we have chosen the base mediated oxidative cyclization reaction of substituted 1° and/or 2° alcohols. This chapter is an extended study of Chapter 3 with similar mechanistic insight where the morphological variance evidenced for the improvement of the catalyst activity along with enhancing its boundary to two component reactions.

4.2.2 Catalytic study of MOP-Am2

Up till now metal free catalysis with POPs have rarely been explored in the accumulated scientific literature. Control oxidation of benzyl alcohol selectively is often considered as a benchmark reaction to study a catalytic reaction. Common strategies usually mandate metal ions along with oxidant like H_2O_2, O_2, O_3 or TBHP etc. Here we have targeted to extend our study in the catalytic synthesis of quinoline and its derivatives *via* oxidative cyclization as model reaction (Scheme 4.2). This reaction was so chosen to minimize the use of precious metal like Ru or toxic chemicals such as pyridine [14,25]. Perhaps, this reaction avoids any kind of toxic oxidant or peroxide as oxidation source. Indeed, environmentally benign base is utilized for the oxidation in presence of reusable MOP-Am2. The components responsible for the transformation like oxidation source, sacrificial agents and catalyst necessities were resolved accordingly and presented. The reaction was optimized by taking *2*-aminobenzyl alcohol and *1*-phenylethanol as model substrates (Table 4.1).

Table 4.1 Reaction condition optimization for the oxidative annulation of alcohols to quinoline. [a]

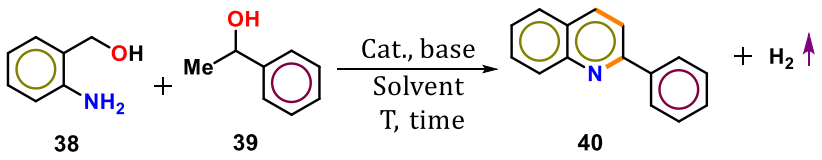

Entry	Cat. wt %	Base (mmol %)	Solvent	Temperature (°C)	Time	**40** % Yield[b]
1	15	KO^{t}Bu (60)	Toluene	110	12 h	93
2	15	KO^{t}Bu (60)	DMF, MeCN	110	12 h	-
3	15	KO^{t}Bu (60)	H_2O	110	12 h	22

4	15	KO^{t}Bu (60)	THF	110	12 h	85
5	15	KO^{t}Bu (60)	1,4-Dioxane	110	12 h	52
6	15	KO^{t}Bu (30)	Toluene	110	12 h	93
7	15	KO^{t}Bu (20)	Toluene	110	12 h	82
8	15	-	Toluene	110	24 h	NR
9	15	K_2CO_3 (30), Cs_2CO_3 (30), Et_3N (30), Bu_3N (30)	Toluene	110	12 h	NR
10	15	NaOH (30)	Toluene	110	12 h	48
11	-	KO^{t}Bu (30)	Toluene	110	24 h	NR
12	10	KO^{t}Bu (30)	Toluene	110	12 h	93
13	8	KO^{t}Bu (30)	Toluene	110	12 h	93
14	6	KO^{t}Bu (30)	Toluene	110	12 h	82
15	8	KO^{t}Bu (30)	Toluene	90	12	93
16	8	KO^{t}Bu (30)	Toluene	80-85	12	93
17	8	KO^{t}Bu (30)	Toluene	70	12	66
18	8	KO^{t}Bu (30)	Toluene	80-85	6 h	93
19	8	KO^{t}Bu (30)	Toluene	80-85	5 h	93
20	8	KO^{t}Bu (30)	Toluene	80-85	4 h	93
21	8	KO^{t}Bu (30)	Toluene	80-85	3 h	93
22	8	KO^{t}Bu (30)	Toluene	80-85	2 h	76

[a] Optimized reaction condition: **38** (0.5 mmol), **39** (0.6 mmol), Solvent = Toluene (1 mL), Cat. = 8% (wt %), base = KO^{t}Bu (30 mol %), T= 80-85 °C, time = 3 h. [b] Isolated yields. NR = No reaction

On optimization with a range of polar and nonpolar solvents, the reaction was found not to proceed with MeCN and DMF (Table 4.1, entry 2). The reaction in aqueous medium yielded approximately 22% (Table 4.1, entry 3) while those in THF and 1,4-dioxane produced quite good yield *i.e.*, approximately 85% and 52% respectively

(Table 4.1, entry 4 & 5). Alcoholic solvents were omitted based on the ability of the reaction media to oxidize the solvents that complicates the overall reaction products. The reaction was further examined with various organic and inorganic bases such as KOH, K_2CO_3, Cs_2CO_3, NaOH, KO^{t}Bu, Et_3N, DBU, DMAP (Table 4.1, entry 6-10) besides their stoichiometry that resulted KO^{t}Bu in 30 mol % to be the optimized condition as well as a sacrificial agent. To confirm the reaction was indeed catalysed by MOP-Am2, we conducted a control experiment with changing the catalyst amount. However, catalyst amount below 8% with respect to **38**, affected the product yield (Table 4.1, entry 11-14). In addition, the 8% of catalyst amount reduced the reaction time to 3 h and decreased the reaction temperature to 80-85 °C (table 4.1, entry 15-22) which signifies that MOP-Am2 promotes the reaction by providing the surface to get the oxidized cyclized product. Without incorporation of MOP-Am2, no reaction changes had been observed even after addition of base for 24 h and vice versa which establishes its essentiality to the reaction condition. (Table 4.1, entry 11 & 8).

4.2.3 Substrate scope study on oxidative annulation

Numbers of methods are known for the synthesis of quinolines using different metal ions. But using a metal free recyclable catalysts is therefore a promising solution towards green and sustainable synthetic development. With the optimal reaction conditions established, the superiority and limitations of MOP-Am2 were examined with a series of varied and distinct substituted alcohols summarized in Table 4.2. Various electron withdrawing/donating and halogen substituted alcohols were reacted and worked well.

Table 4.2 eventually showed that, for R^1=H, both the *p*-alkyl and *p*-alkoxy substituent on **5** yields 96% (Table 4.2, **37b** & **37c**) of the corresponding products in comparison to the yield of 93 % for 1-phenylethanol. This is attributed to the increase in reactivity of the keto-enol form of the corresponding carbonyl form of **36** because of the electron donating substituent. In addition, the *m*-alkyl substituted **36** did not hamper the overall reactivity and retains its productivity (Table 4.2, **37d**). This suggested no major positional isomeric effect is present in the reaction condition. The halogenated **36** also showed good to excellent yields (Table 4.2, **37e-37h**). The more electronegative *p*-fluoro substitution possessed comparatively lower yield than that

of *p*-choro, *p*-bromo or *p*-iodo. The electron withdrawing substituent on **36** exhibited relatively lower yield (Table 4.2, **37i** & **37j**) which might appear for lowering in reactivity of corresponding carbonyl form of **36**.

Table 4.2 Substrate scope of various substituted alcohols towards annulation.[a][b]

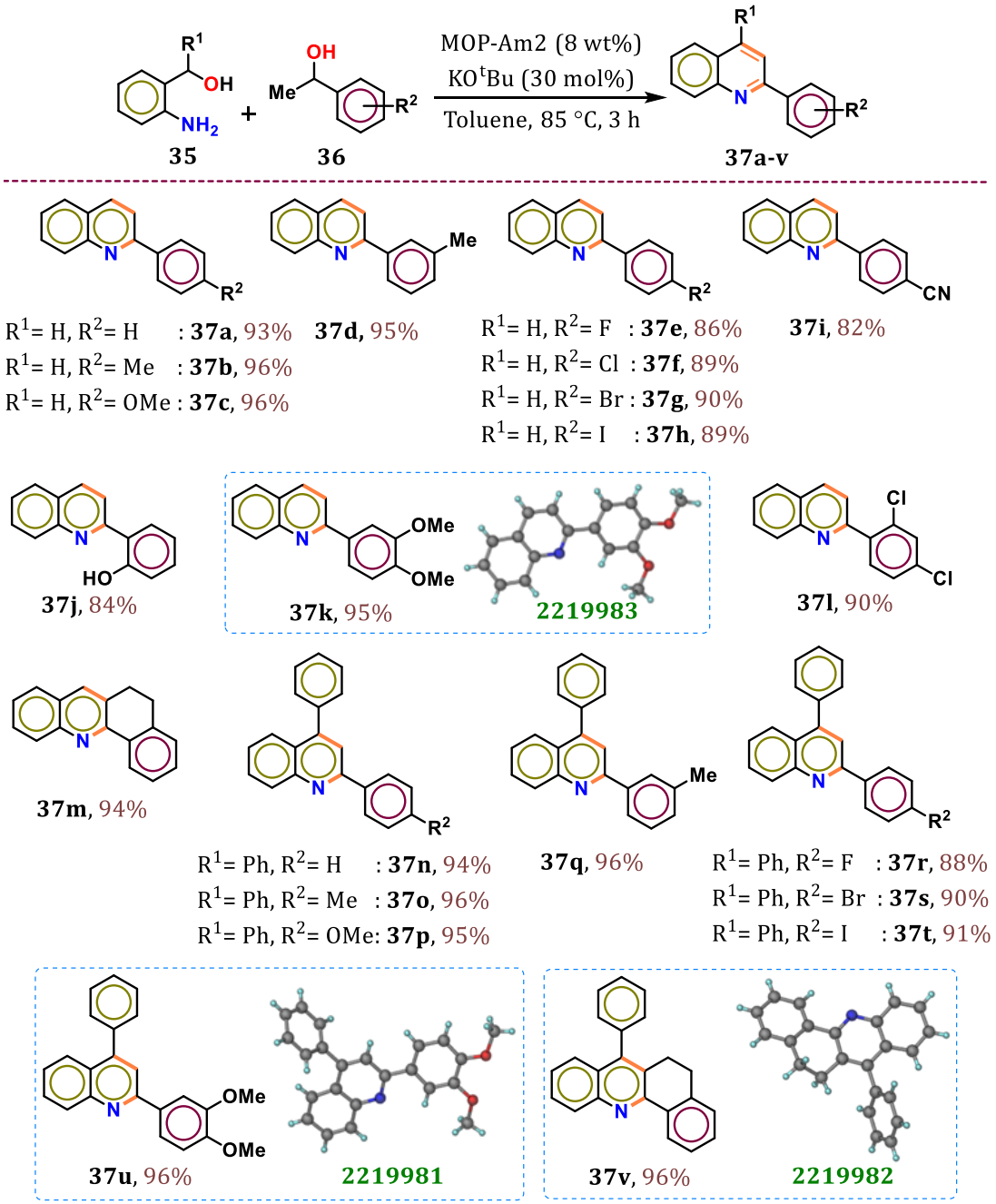

[a] Optimized reaction condition: **35** (0.5 mmol), **36** (0.6 mmol), Solvent = Toluene (1-2 mL), Cat. = 8% (wt %), base = KO^{t}Bu (30 mol %), T = 80-85 °C, time= 3 h. [b] Isolated yields. CCDC number (green)

Further investigation of multiple substitutions on **36** were reported with corresponding products in excellent yield (Table 4.2, **37k & 37l**). Interestingly, this protocol also validated for cyclic aliphatic secondary alcohol (Table 4.2, **37m**) with excellent productivity of 94 %. This result contradicts Sotains' Re-catalyst that fails to produce quinoline from aliphatic alcohols [30]. Alongside with R^1=Ph, the reaction did not suffer any obstacles for the formation of quinolines. In fact, the overall reactivity remains unchanged and it followed the similar trend of product formation (Table 4.2, **37n-37v**) but slightly in lower reaction time. This is due to the fact that the phenyl substitution at benzylic position made **35** more prone to form corresponding carbonyl compound and hence decreased the reaction time.

4.2.4 Gram scale synthesis

Accessing the current protocol to gram scale synthesis, we scale up the reaction by taking 2-aminobenzyl alcohol, **38** and 1-(*p*-anisyl)ethanol, **41** as model substrate (Scheme 4.3); and investigated the green matrices of the reaction. The reaction afforded around 88% desired conversion as the reaction time completed. The E-factor after the isolation of the product was calculated to be 4.367 kg waste/kg product; while the calculated carbon efficiency was 100%. This finding was further supported by determining the carbon emission to the environment during the reaction using modified Walkley-Black redox titration method [26]. It is the ratio of the carbon contents present in the product side to that of the reactant side. Notably, the experiment also proves no carbon emission or loss throughout the process thereby making the overall protocol affordable, sustainable, and environmentally benign.

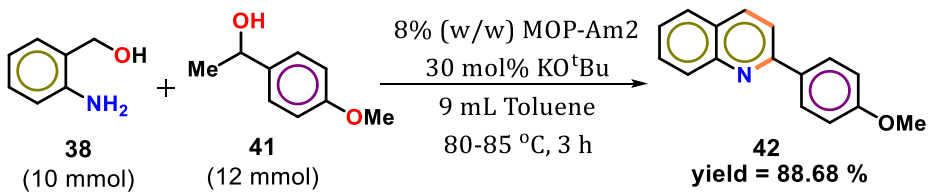

38 (10 mmol) + **41** (12 mmol) → **42** yield = 88.68 %

Green chemistry matrices

i. Atom economy= 85.43%
ii. Atom efficiency= 75.76%
iii. Carbon balance= 99.27%
iv. Reaction mass efficiency= 75. 81%
v. Excess Reactant Factor= 1.04
vi. E-factor= 4.367 kg waste/1 kg product

Scheme 4.3 Gram scale synthesis of 2-(*p*-anisyl)quinoline

4.2.5 Mechanism study

To understand the importance of the extended π-conjugation, we carried out reactions of a few selective substrates with a monomeric unit, MOP-Am2-m keeping all other reaction conditions consistent. Comparing the yields obtained in both the catalytic systems (Table 4.3), the low yield under the monomeric system upholds the imperative role of the extended π-conjugation along with electron rich nitrogen centres.

Table 4.3 Catalytic conversion comparison of both MOP-Am2 and MOP-Am2-m under same reaction condition.

Entry	Catalyst	% Conversion
37a	MOP-Am2	93%
	MOP-Am2-m	12%
37c	MOP-Am2	96%
	MOP-Am2-m	15%
37d	MOP-Am2	86%
	MOP-Am2-m	4%
37g	MOP-Am2	90%
	MOP-Am2-m	7%
37i	MOP-Am2	82%
	MOP-Am2-m	trace
37j	MOP-Am2	84%
	MOP-Am2-m	trace
20l	MOP-Am2	90%
	MOP-Am2-m	10%
37p	MOP-Am2	96%
	MOP-Am2-m	13%
37u	MOP-Am2	96%
	MOP-Am2-m	12%
37v	MOP-Am2	96%
	MOP-Am2-m	14%

It is affirmative to mention that increasing the overall electronic conjugation lowers the band gap more than that of the monomeric unit [26]. This provides better electron accessibility from MOP-Am2 for interacting with the α-carbon of the alcohols that make the Cα–H bond labile. Interestingly in absence of a base, such activation of Cα–H could not be found as the probability of weak interaction of MOP-Am2 is now predominant towards O–H of alcohols. Hence the reaction does not proceed. However, upon addition of base, the alcohol exists as alkoxide and hence the interaction probability of MOP-Am2 is now shifted towards α-carbon forming corresponding carbonyl intermediate that triggered the hydrogen evolution [26]. The evolution of H_2 was further confirmed with *in-situ* reduction reaction of diphenylacetylene taking **39** as hydrogen source. The formation of *cis*-Stilbene was confirmed with ^{1}H and ^{13}C NMR analysis as described in Chapter 3.

To ascertain the actual mechanism, we traced the intermediates, by means of ^{1}H NMR titration method taking **38** and **39** as initial substrate and plotted the ^{1}H NMR spectra for each crude reaction mixture under a certain period of time (Figure 4.4). The stacked ^{1}H NMR spectra suggested that at the initial 5 min, both the substrate molecule started oxidizing to their corresponding carbonyl compounds.

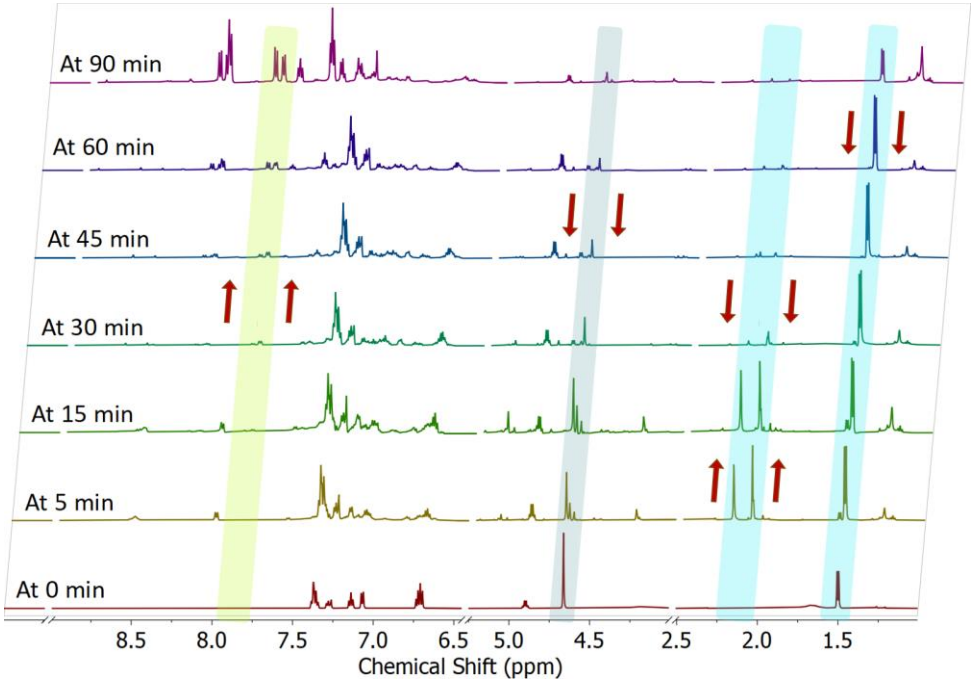

Figure 4.4 Overlay ^{1}H NMR (600 MHz, $CDCl_3$, 298 K) spectra for the annulation of 2-aminobenzyl alcohol and 1-phenylethanol at various interval of time

At the initial stage, the conversion of **39** to acetophenone is faster than that of **38** because of the absence of $-NH_2$. As a result, the proton signal for $-CH_3$ of **39** at 1.50 ppm started shifting to 2.19 ppm whereas the same was barely observed for 2-aminobenzaldehyde formation. Following it contradicted the possibility of aldol condensation, instead the acetophenone started reacting to $-NH_2$ forming an imine intermediate along with its own oxidation. As a result, we found a singlet for $-N=C-CH_3$ at 2.08 ppm. This intermediate then made the oxidation of the 1^0 alcohol faster due to obvious reasons of presence of an electron withdrawing group. With time, the intensity started to diminish of the imine intermediate to the aldehyde center took place. As a result, two doublets at 7.84 and 7.89 ppm started appearing for the newly formed C=C double bond with the elimination of H_2O.

The cyclization step of the reaction was so fast that all the oxidation, elimination, and cyclization took place simultaneously. As a result, the ^1H NMR signals for the oxidized alcohols were barely visible after 30 min of reaction time and the reaction continued till the completion. Based on the experimental evidences, the plausible mechanism associated with the oxidative annulation of alcohols is depicted in Figure 4.5.

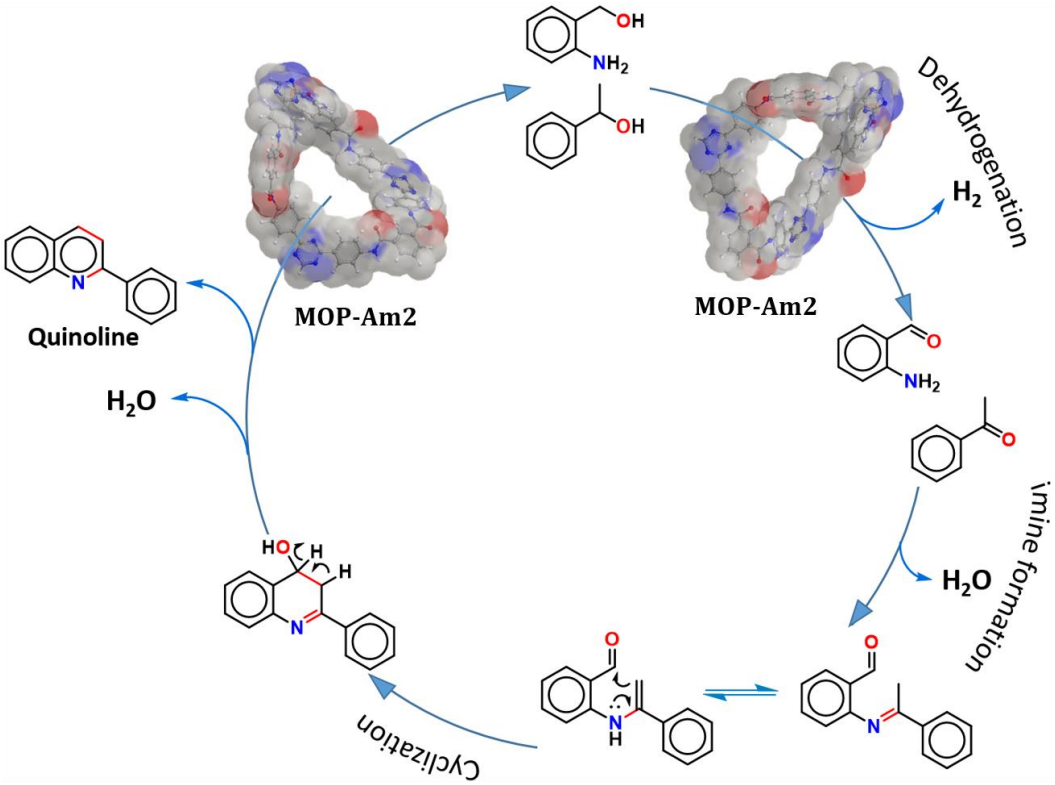

Figure 4.5 Plausible mechanistic pathway involved in the catalytic conversion to quinoline driven by morphologically modified MOP-Am2

4.2.6 Catalyst reusability and stability

The high thermal and chemical stability of MOP-Am2 also dealt with the major concern about a catalyst in any domain of reactions, *i.e.*, recyclability and efficiency. Interestingly MOP-Am2 was examined and utilized for seven consecutive cycles (Figure 4.6a).

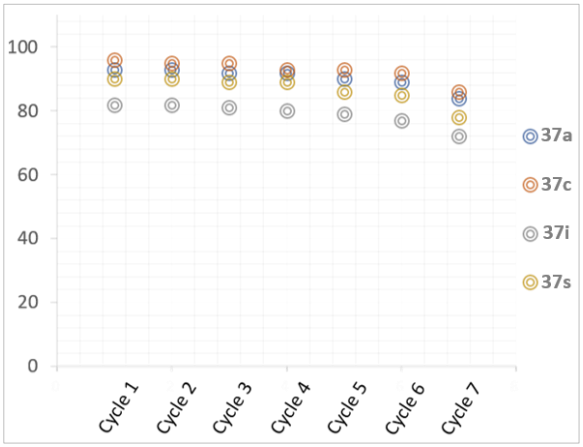

Figure 4.6 Catalytic reusability of MOP-Am2 for up to seven consecutive cycles with four representative substrates and their corresponding % yields in abscissa

The reused catalyst was recovered *via* filtration, washed several times and characterized with PXRD analysis. It is evident from Figure 4.7 that no such drastic structural integrity changes have been observed in the PXRD pattern while comparing the reused MOP-Am2 after seven catalytic cycle with the pristine material. However, a very minute variation in its catalytic performance was observed that might attributes due to the deactivation of the active sites of MOP-Am2 over multiple catalytic cycles.

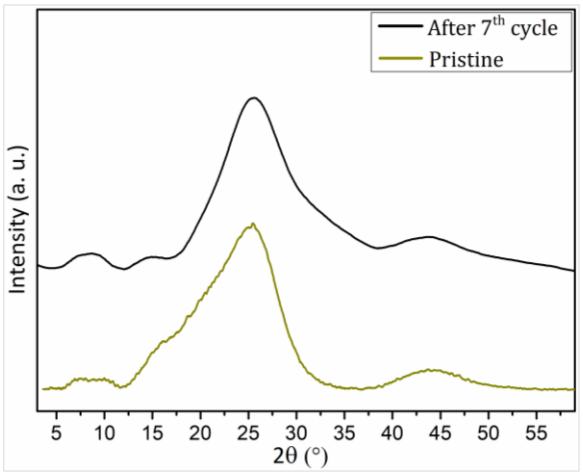

Figure 4.7 Overlay PXRD patterns of reused catalyst and the pristine MOP-Am2

4.3 Summary

Morphological modification has been demonstrated here to accomplish the annulation of alcohols under mild reaction conditions along with the evolution of hydrogen, on a gram scale synthesis. The excess nitrogen and extended π-conjugation in MOP-Am2 acts as driving force for the formation of carbonyl intermediate making the benzylic C–H bond labile. The evolution of hydrogen in the reaction protocol was established by the *in-situ* reduction of diphenylacetylene. The ^{1}H NMR titration study was designed to understand the mechanistic insights of the reaction which confirmed the involvement of the enamine intermediate, drove the cyclization for heteroaromatic annulation. The affordability and sustainability of the protocol was further demonstrated by revealing the green matrices determination of the scale up synthesis. The E-factor was calculated to be 4.367 kg waste/kg product; while the calculated carbon efficiency was 99.27%. The liberated hydrogen over designed microporous organic polymer (MOP-Am2) opens up an added facet of its applications which is discussed in the next chapter.

4.4 Experimental Section

4.4.1 Materials and methods

All chemicals employed in this study are purchased from commercial sources (Sigma Aldrich, Alfa Aesar and Merck) and used as such without further purification until otherwise mentioned.

The porosity and rigidity of morphology modified MOP-Am2 were measured recording the N_2 adsorption-desorption isotherm of it at Quantachrome (Version 3.0) surface area analyzer. The liquid nitrogen used in the measurement was of ultra-high purity (99.999% pure) and the refrigerated bath of liquid nitrogen (77 K) further controls the temperature during the process.

Field emission scanning electron microscope (FESEM) images were recorded in Gemini 500 FESEM (software: SmartSEm User Interface) and transmission electron microscope (TEM) images were recorded in JEOL JEM 2100 at an accelerating voltage of 200 kV to examine the surface and bulk morphology.

The powder X-ray diffraction (PXRD) patterns were recorded in D8 ADVANCE X-ray using monochromated Cu Kα (λ = 1.542 Å) radiation from Bruker. Single crystal X-ray diffractions were collected on a Bruker SMART APEX-II CCD diffractometer using Mo Kα (λ =0.71073 Å) radiation. All the structures were solved and refined using SHELXL.

The progress of the reactions was monitored by TLC using TLC silica gel F254 250 μm precoated-plates from Merck and the product formation were confirmed by NMR spectrometer (Bruker AVANCE NEO NMR SPECT. 400 MHz), (JEOL ECS-400, DELTA, VERSION-4.3.6), (Bruker, AVANCE III HD 600 MHz) and HRMS (Xevo G2-XS QTOF (Waters) mass spectrometer using electron spray ionization mass).

4.4.2 Modified synthesis of MOP-Am2

To construct the morphologically modified MOP-Am2; in a 250 mL two neck round bottom flask, an amount of 1 mmol of TAPT was dissolved in 25 mL of dry 1,4-dioxane and kept in an ice cold water bath and additionally 3 mmol of Et_3N was added in it. A solution of 1 mmol BTCl in dry 1,4-dioxane (10 mL) was slowly added over a period of 2 h in nitrogenous environment and left with continuous stirring for 12 h. Special care was taken while performing the reaction as it liberates corrosive HCl gas during condensation. The liberated HCl gas was trapped with Et_3N which was then easily removed during filtration. The collected precipitate was then added to 50 mL of acetonitrile and refluxed for another 24 h. The reaction was then allowed to cool to room temperature and filtered. The obtained precipitate was washed with acetone and dry DMF to avoid unreacted impurities and dried under vacuum at 100 °C for 24 h to remove the surface captured solvent molecules and then characterized.

4.4.3 General synthetic procedure for the annulation of alcohols

In a 20 mL Schlenk tube 0.5 mmol of **18**, 0.6 mmol of **19**, 30 mol % of KO^tBu, 8 wt % of MOP-Am2, and 1-2 mL of toluene were added and heated at 80-85 °C for 3 h. The reactions were monitored using TLC. The desired products were isolated by column chromatography using varied ethyl acetate:*n*-hexane mixture. The isolated products were characterized by ^1H & ^{13}C NMR spectroscopy and HRMS.

4.4.4 Procedure for gram scale synthesis of annulation of alcohols

In a 30 mL Schlenk tube 10 mmol of **15**, 12 mmol of **22**, 30 mol % of KO^{t}Bu, 8 wt % of MOP-Am2,) and 9 mL of toluene were added and heated at 80-85 ^{0}C for 3 h. The reactions were monitored using TLC. The desired products, **23** were isolated by column chromatography using 6% ethyl acetate:*n*-hexane mixture. The isolated products were characterized by ^{1}H and ^{13}C NMR spectroscopy and HRMS.

4.4.5 Determination of the carbon efficiency

The carbon efficiency or total organic carbon (OC) during the reaction has been calculated using modified Walkley-Black method of redox titration discussed in Chapter 3. 1N dichromate solution was taken as a digester as well as an oxidizing agent that breaks down the organic scaffolds and convert it to CO_2. Remaining dichromate solution was titrated against 0.5M $Fe(NH_4)_2(SO_4)_2$ solution. Subtraction of the titrant value of 0.5M $Fe(NH_4)_2(SO_4)_2$ solution during the organic transformation reaction from the blank titrant value results the quantity of dichromate solution involved during the oxidation of the organic moieties to CO_2.

General procedure for the redox titration was mentioned in Chapter 3. For the blank sample, the titrant value was found to be 18.9 mL. The concordant titrant values in Scheme 4.3, before and after the reaction, are tabulated below (Table 4.4).

Table 4.4 Carbon efficiency or total organic carbon (OC) in Scheme 4.3.

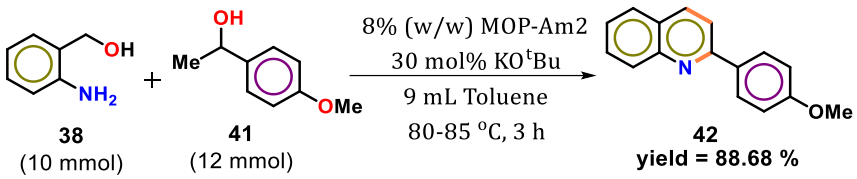

Entry	Weight Taken (mg)	Before Reaction		After Reaction		%OC
		Titrant value of 0.5M $Fe(NH_4)_2(SO_4)_2$ (mL)	OC content quantity on reactant side (mg)	Titrant value of 0.5M $Fe(NH_4)_2(SO_4)_2$ (mL)	OC content quantity on reactant side (mg)	
Scheme 4.3	30	5.2	20.55	5.3	20.40	99.27

The redox reaction involved is-

$$2\ Cr_2O_7^{2-} + 3\ C^0 + 16\ H^+ \longleftrightarrow 4\ Cr^{3+} + 3\ CO_2 + 8\ H_2O \qquad \text{------ (i)}$$

Therefore, 1 mL of 1N $K_2Cr_2O_7$ solution = 0.003 g of Carbon.

$$\text{Thus, \%OC} = \frac{(B-S)\times M[Fe(II)]\times 0.003\times 100}{\text{Amount of test sample in g}} \qquad \text{---------- (ii)}$$

Where, B= Titrant volume of blank solution, i.e. without sample

S= Titrant volume for Substrate solution

M[Fe(II)]= Concentration of $Fe(NH_4)_2(SO_4)_2$ solution

4.4.6 Method to cultivate the crystal 37k, 37u and 37v

~50 mg of 8m was dissolved in 1 mL of $CHCl_3$ in a glass vial and kept for slow evaporation. Yellowish plate and block shape crystals of the desired products were observed after few days that were characterized with single crystal X-ray crystallography.

4.5 Spectral Data Analysis

2-Phenylquinoline:

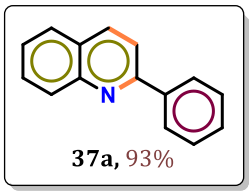

37a, 93%

^{1}H NMR (400 MHz, $CDCl_3$) δ (ppm): 8.20–8.12 (m, 4H), 7.82 (d, *J* = 8.6 Hz, 1H), 7.77 (d, *J* = 8.1 Hz, 1H), 7.70 (ddd, *J* = 8.4, 6.9, 1.4 Hz, 1H), 7.53–7.41 (m, 4H). ^{13}C{^{1}H} NMR (101 MHz, $CDCl_3$) δ (ppm): 157.5, 148.4, 139.8, 136.9, 129.9, 129.8, 129.4, 129.0, 127.7, 127.6, 127.3, 126.4, 119.1. HRMS (ESI+) m/z calcd $[M+H]^+$: 206.0969, found 206.0965.

***2-(p-Tolyl)quinoline*:**

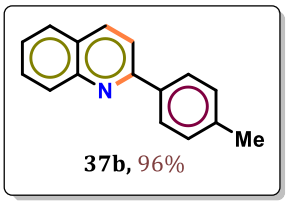

37b, 96%

^{1}H NMR (400 MHz, $CDCl_3$) δ (ppm): 8.15 (d, *J* = 8.5 Hz, 1H), 8.12 (d, *J* = 8.7 Hz, 1H), 8.05 (d, *J* = 8.2 Hz, 2H), 7.80 (d, *J* = 8.6 Hz, 1H), 7.77–7.74 (m, 1H), 7.68 (ddd, *J* = 8.4, 6.9, 1.4 Hz, 1H), 7.46 (ddd, *J* = 8.0, 6.9, 1.1 Hz, 1H), 7.30 (d, *J* = 8.0 Hz, 2H), 2.40 (s, 3H). ^{13}C{^{1}H} NMR (101 MHz, $CDCl_3$) δ (ppm): 157.4, 148.4, 139.5, 137.0, 136.8, 129.8, 129.7, 127.6, 127.2, 126.2, 119.0, 21.5. HRMS (ESI+) m/z calcd $[M+H]^+$: 220.1126, found 220.1121.

***2-(4-Methoxyphenyl)quinoline*:**

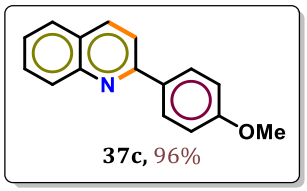

37c, 96%

^{1}H NMR (400 MHz, $CDCl_3$) δ (ppm): 8.18 (d, *J* = 8.7 Hz, 1H), 8.14 (d, *J* = 8.8 Hz, 3H), 7.84 (d, *J* = 8.6 Hz, 1H), 7.80 (d, *J* = 8.2 Hz, 1H), 7.71 (t, *J* = 7.7 Hz, 1H), 7.50 (t, *J* = 7.0 Hz, 1H), 7.05 (d, *J* = 8.9 Hz, 2H), 3.89 (s, 3H). ^{13}C{^{1}H} NMR (101 MHz, $CDCl_3$) δ (ppm): 160.8, 156.9, 148.3, 136.6, 129.6, 129.5, 128.9, 127.4, 126.9, 125.9, 118.6, 114.2, 55.4. HRMS (ESI+) m/z calcd $[M+H]^+$: 236.1075, found 236.1074.

***2-(m-Tolyl)quinoline*:**

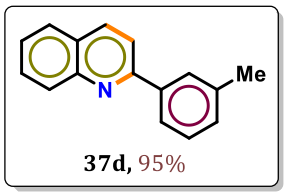

37d, 95%

^{1}H NMR (400 MHz, $CDCl_3$) δ (ppm): 8.17 (t, *J* = 8Hz, 2H), 8.00 (s, 1H), 7.91 (d, *J* = 7.7 Hz, 1H), 7.83 (d, *J* = 8.6 Hz, 1H), 7.78 (d, *J* = 8.1 Hz, 1H), 7.70 (ddd, *J* = 8.4, 6.9, 1.4 Hz, 1H), 7.51–7.47 (m, 1H), 7.40 (t, *J* = 7.6 Hz, 1H), 7.26 (d, *J* = 7.5 Hz, 1H), 2.46 (s, 3H). ^{13}C{^{1}H} NMR (101 MHz, $CDCl_3$) δ (ppm): 157.6, 148.2, 139.6, 138.5, 136.7, 130.1, 129.7, 129.6, 128.7, 128.2, 127.4, 127.1, 126.1, 124.7, 119.1, 21.6. HRMS (ESI+) m/z calcd $[M+H]^+$: 220.1126, found 220.1124.

***2-(4-Fluorophenyl)quinoline*:**

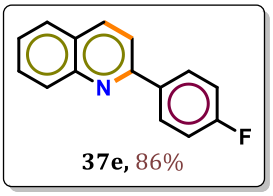

37e, 86%

^{1}H NMR (400 MHz, $CDCl_3$) δ (ppm): 8.13 (t, *J* = 8.2 Hz, 4H), 7.76 (t, *J* = 6.5 Hz, 2H), 7.70 (t, *J* = 7.5 Hz, 1H), 7.49 (t, *J* = 7.4 Hz, 1H), 7.17 (t, *J* = 8.6 Hz, 2H). ^{13}C{^{1}H} NMR (125 MHz, $CDCl_3$) δ (ppm): 163.95 (d, *J* = 249.0 Hz), 156.3, 148.4, 137.0, 135.9 (d, J_{C-F} = 2.9 Hz), 129.9, 129.8, 129.54 (d, J_{C-F} = 8.5 Hz), 127.6, 127.2, 126.5, 118.7, 115.87 (d, J_{C-F} = 21.8 Hz). HRMS (ESI+) m/z calcd $[M+H]^+$: 224.0875, found 240.0881.

***2-(4-Chlorophenyl)quinoline*:**

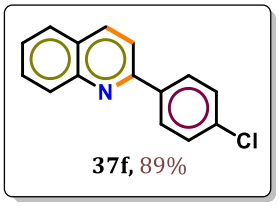

37f, 89%

^{1}H NMR (400 MHz, $CDCl_3$) δ (ppm): 8.20 (d, *J* = 8.6 Hz, 1H), 8.15 (d, *J* = 8.5 Hz, 1H), 8.13–8.07 (m, 2H), 7.81 (d, *J* = 8.5 Hz, 2H), 7.73 (ddd, *J* = 8.4, 6.9, 1.4 Hz, 1H), 7.53 (ddd, *J* = 8.1, 7.0, 1.0 Hz, 1H), 7.51–7.46 (m, 2H). ^{13}C{^{1}H} NMR (101 MHz, $CDCl_3$) δ (ppm): 156.1, 148.4, 138.2, 137.1, 135.7, 130.0, 129.8, 129.2, 129.0, 127.7, 127.4, 126.7, 118.7. HRMS (ESI+) m/z calcd $[M+H]^+$: 240.0580, found 240.0575.

***2-(4-Bromophenyl)quinoline*:**

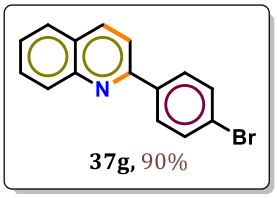

37g, 90%

^{1}H NMR (600 MHz, $CDCl_3$) δ (ppm): 8.23 (d, *J* = 8.6 Hz, 1H), 8.16 (d, *J* = 8.5 Hz, 1H), 8.06 (d, *J* = 8.3 Hz, 2H), 7.86–7.81 (m, 2H), 7.74 (t, *J* = 7.6 Hz, 1H), 7.65 (d, *J* = 8.3 Hz, 2H), 7.54 (t, *J* = 7.4 Hz, 1H). ^{13}C{^{1}H} NMR (151 MHz, $CDCl_3$) δ (ppm): 156.2, 148.4, 138.67, 137.2, 132.1, 130.0, 129.9, 129.3, 127.7, 127.4, 126.7, 124.1, 118.7. HRMS (ESI+) m/z calcd $[M+H]^+$: 284.0074, found 284.0067.

***2-(4-Iodophenyl)quinoline*:**

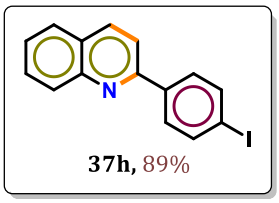

37h, 89%

^{1}H NMR (400 MHz, $CDCl_3$) δ (ppm): 8.22 (d, *J* = 8.6 Hz, 1H), 8.16 (d, *J* = 8.5 Hz, 1H), 7.92 (d, *J* = 8.4 Hz, 2H), 7.89–7.80 (m, 4H), 7.73 (t, *J* = 7.2 Hz, 1H), 7.54 (t, *J* = 7.4 Hz, 1H). ^{13}C{^{1}H} NMR (125 MHz, $CDCl_3$) δ (ppm): 156.3, 148.5, 139.2, 138.2, 137.2, 130.1, 129.9, 129.5, 127.7, 127.5, 126.7, 118.6, 96.1. HRMS (ESI+) m/z calcd $[M+H]^+$: 331.9936, found 331.9941.

***4-(Quinolin-2-yl)benzonitrile*:**

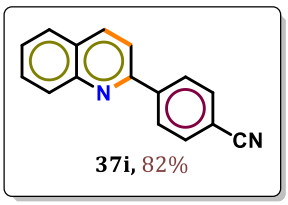

37i, 82%

^{1}H NMR (400 MHz, $CDCl_3$) δ (ppm): 8.31–8.27 (m, 3H), 8.18 (d, *J* = 8.5 Hz, 1H), 7.87 (t, *J* = 9.0 Hz, 2H), 7.84–7.79 (m, 2H), 7.77 (ddd, *J* = 8.4, 6.9, 1.4 Hz, 1H), 7.58 (ddd, *J* = 8.0, 7.0, 1.1 Hz, 1H). ^{13}C{^{1}H} NMR (101 MHz, $CDCl_3$) δ (ppm): 155.1, 148.5, 143.9, 137.5, 132.8, 130.3, 130.1, 128.3, 127.7, 127.3, 118.8, 112.9.

***2-(2-Hydroxyphenyl)quinoline*:**

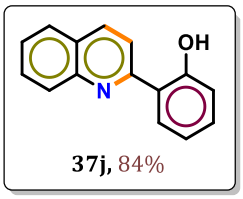

37j, 84%

^{1}H NMR (400 MHz, $CDCl_3$) δ (ppm): 14.91 (s, 1H), 8.28 (d, *J* = 8.9 Hz, 1H), 7.96 (dd, *J* = 8.0, 1.5 Hz, 1H), 7.83 (d, *J* = 8.1 Hz, 1H), 7.83 (d, *J* = 8.1 Hz, 1H), 7.75 (ddd, *J* = 8.4, 7.0, 1.4 Hz, 1H), 7.58–7.53 (m, 1H), 7.37 (ddd, *J* = 8.5, 7.2, 1.6 Hz, 1H), 7.10 (dd, *J* = 8.3, 1.2 Hz, 1H), 6.99–6.94 (m, 1H). ^{13}C{^{1}H} NMR (101 MHz, $CDCl_3$) δ (ppm): 161.2, 158.2, 145.0, 137.8, 132.2, 130.7, 127.8, 127.7, 127.1, 126.9, 126.7, 119.2, 118.9, 118.9, 117.4. HRMS (ESI+) m/z calcd $[M+H]^+$: 222.0918, found 222.0921.

***2-(3,4-Dimethoxyphenyl)quinoline*:**

^{1}H NMR (400 MHz, $CDCl_3$) δ (ppm): 8.15 (d, *J* = 8.3 Hz, 2H), 7.88 (d, *J* = 2.0 Hz, 1H), 7.86–7.77 (m, 2H), 7.68 (ddd, *J* = 10.4, 8.2, 4.4 Hz, 2H), 7.52–7.46 (m, 1H), 6.98 (d, *J* =

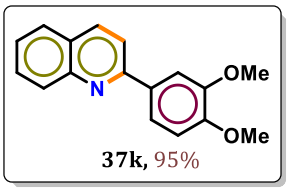

37k, 95%

8.4 Hz, 1H), 4.04 (s, 3H), 3.94 (s, 3H). $^{13}C\{^{1}H\}$ NMR (101 MHz, $CDCl_3$) δ (ppm): 157.0, 150.5, 149.5, 148.4, 136.8, 132.7, 129.7, 129.6, 127.6, 127.1, 126.1, 120.4, 118.7, 111.2, 110.5, 56.2, 56.1. HRMS (ESI+) m/z calcd $[M+H]^+$: 266.1181, found: 266.1178.

***2-(2,4-Dichlorophenyl)quinoline*:**

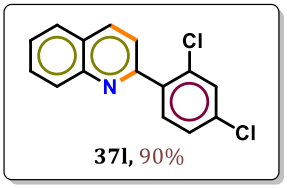

37l, 90%

^{1}H NMR (400 MHz, $CDCl_3$) δ (ppm) : 8.22 (d, *J* = 8.5 Hz, 1H), 8.16 (d, *J* = 8.4 Hz, 1H), 7.87 (d, *J* = 8.1 Hz, 1H), 7.75 (ddd, *J* = 13.6, 7.7, 4.1 Hz, 2H), 7.67 (d, *J* = 8.3 Hz, 1H), 7.59 (ddd, *J* = 8.1, 7.0, 1.1 Hz, 1H), 7.53 (d, *J* = 2.0 Hz, 1H), 7.40 (dd, *J* = 8.3, 2.1 Hz, 1H). $^{13}C\{^{1}H\}$ NMR (101 MHz, $CDCl_3$) δ (ppm): 156.5, 148.3, 138.3, 136.0, 135.4, 133.3, 132.8, 130.0, 129.8, 127.8, 127.4, 127.2, 122.7. HRMS (ESI+) m/z calcd $[M+H]^+$: 274.0190, found 274.0194.

***5,6-Dihydrobenzo[c]acridine*:**

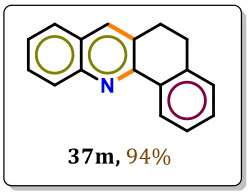

37m, 94%

^{1}H NMR (400 MHz, $CDCl_3$) δ (ppm): 8.60 (dd, *J* = 7.7, 1.2 Hz, 1H), 8.15 (d, *J* = 8.4 Hz, 1H), 7.91 (s, 1H), 7.74 (d, *J* = 8.1 Hz, 1H), 7.66 (ddd, *J* = 8.4, 6.9, 1.4 Hz, 1H), 7.50–7.42 (m, 2H), 7.38 (td, *J* =7.4, 1.5 Hz, 1H), 7.28 (d, *J* = 7.3 Hz, 1H), 3.13 (dd, *J* = 8.0, 5.8 Hz, 2H), 3.02 (dd, *J* = 8.3, 5.4 Hz, 2H). $^{13}C\{^{1}H\}$ NMR (101 MHz, $CDCl_3$) δ (ppm): 153.6, 147.8, 139.6, 134.9, 133.8, 130.7, 129.8, 129.6, 128.8, 128.1, 128.0, 127.5, 127.1, 126.2, 126.2, 29.0, 28.6. HRMS (ESI+) m/z calcd $[M+H]^+$: 232.1126, found 232.1122.

***2,4-Diphenylquinoline*:**

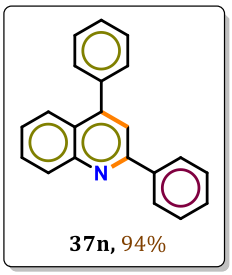

37n, 94%

^{1}H NMR (400 MHz, $CDCl_3$) δ (ppm): 8.28 (d, *J* = 8.1 Hz, 1H), 8.25–8.21 (m, 2H), 7.93 (dd, *J* = 8.4, 1.0 Hz, 1H), 7.84 (s, 1H), 7.75 (ddd, *J* = 8.4, 6.8, 1.4 Hz, 1H), 7.60–7.46 (m, 9H). $^{13}C\{^{1}H\}$ NMR (101 MHz, $CDCl_3$) δ (ppm): 157.0, 149.3, 149.0, 139.8, 138.6, 130.3, 129.7, 129.7, 129.5, 129.0, 128.7, 128.5, 127.7, 126.5, 125.9, 125.8, 119.5. HRMS (ESI+) m/z calcd $[M+H]^+$: 282.1282, found 282.1285.

***4-Phenyl-2-(p-tolyl)quinoline*:**

^{1}H NMR (400 MHz, $CDCl_3$) δ (ppm): 8.27 (d, *J* = 8.4 Hz, 1H), 8.14 (d, *J* = 8.1 Hz, 2H), 7.92 (d, *J* = 8.4 Hz, 1H), 7.83 (s, 1H), 7.77–7.72 (m, 1H), 7.64–7.51 (m, 5H), 7.47 (ddd,

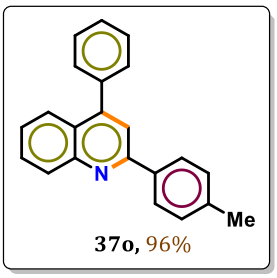

37o, 96%

J = 8.2, 6.9, 1.2 Hz, 1H), 7.36 (d, *J* = 7.9 Hz, 2H), 2.46 (s, 3H). $^{13}C\{^{1}H\}$ NMR (101 MHz, $CDCl_3$) δ (ppm): 157.0, 149.2, 149.0, 139.5, 138.6, 137.0, 130.2, 129.7, 129.6, 128.7, 128.5, 127.6, 126.3, 125.8, 125.7, 119.3, 21.5. HRMS (ESI+) m/z calcd $[M+H]^+$: 296.1439, found 296.1436.

***2-(4-Methoxyphenyl)-4-phenylquinoline*:**

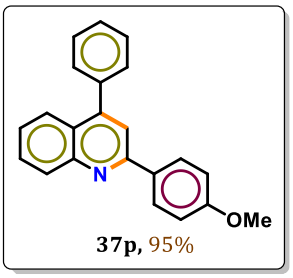

37p, 95%

^{1}H NMR (400 MHz, $CDCl_3$) δ (ppm): 8.21 (d, *J* = 8.4 Hz, 1H), 8.19–8.14 (m, 2H), 7.88 (d, *J* = 7.8 Hz, 1H), 7.78 (s, 1H), 7.71 (ddd, *J* = 8.3, 6.9, 1.3 Hz, 1H), 7.61–7.48 (m, 5H), 7.48–7.42 (m, 1H), 7.11 – 6.98 (m, 2H), 3.89 (s, 3H). $^{13}C\{^{1}H\}$ NMR (101 MHz, $CDCl_3$) δ (ppm): 161.1, 156.6, 149.2, 149.0, 138.7, 132.4, 130.1, 129.8, 129.6, 128.8, 128.5, 126.1, 125.8, 125.7, 119.1, 114.4, 55.6. HRMS (ESI+) m/z calcd $[M+H]^+$: 312.1388, found 312.1386.

***4-Phenyl-2-(m-tolyl)quinoline*:**

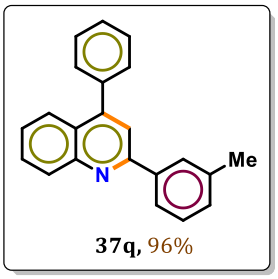

37q, 96%

^{1}H NMR (400 MHz, $CDCl_3$) δ (ppm): 8.29 (d, *J* = 8.1 Hz, 1H), 8.08 (s, 1H), 8.00 (d, *J* = 7.8 Hz, 1H), 7.93 (dd, *J* = 8.4, 0.8 Hz, 1H), 7.84 (s, 1H), 7.75 (ddd, *J* = 8.3, 6.9, 1.4 Hz, 1H), 7.61–7.41 (m, 7H), 7.31 (d, *J* = 7.5 Hz, 1H), 2.51 (s, 3H). $^{13}C\{^{1}H\}$ NMR (101 MHz, $CDCl_3$) δ (ppm): 157.2, 149.2, 149.0, 139.8, 138.6, 130.3, 130.3, 129.7, 129.6, 128.9, 128.7, 128.5, 128.4, 126.4, 125.9, 125.8, 124.9, 119.6, 21.7. HRMS (ESI+) m/z calcd $[M+H]^+$: 296.1439, found 296.1436.

***2-(4-Fluorophenyl)-4-phenylquinoline*:**

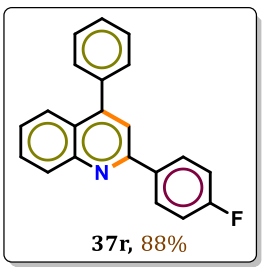

37r, 88%

^{1}H NMR (400 MHz, $CDCl_3$) δ (ppm): 8.28 –8.23 (m, 1H), 8.21 (dd, *J* = 8.7, 5.5 Hz, 2H), 7.91 (d, *J* = 8.4 Hz, 1H), 7.78 (s, 1H), 7.74 (t, *J* = 7.7 Hz, 1H), 7.64–7.50 (m, 5H), 7.48 (t, *J* = 7.6 Hz, 1H), 7.27–7.15 (m, 2H). $^{13}C\{^{1}H\}$ NMR (101 MHz, $CDCl_3$) δ (ppm): 163.9 (d, *J* = 248.9 Hz), 155.9, 149.5, 148.9, 138.5, 135.9 (d, *J* = 3.0 Hz), 130.2, 129.8, 129.7, 129.6 (d, *J* = 8.3 Hz), 128.8, 128.6, 126.5, 125.8, 125.8 (d, *J* = 2.2 Hz), 119.1, 115.9 (d, *J* = 21.6 Hz). HRMS (ESI+) m/z calcd $[M+H]^+$: 300.1188, found 300.1186.

***2-(4-Bromoyphenyl)-4-phenylquinoline*:**

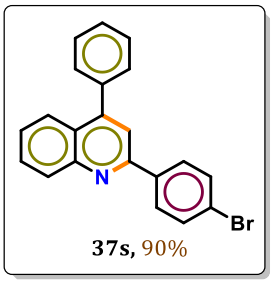

37s, 90%

^{1}H NMR (600 MHz, $CDCl_3$) δ (ppm): 8.22 (d, *J* = 8.4 Hz, 1H), 8.09 (d, *J* = 8.3 Hz, 2H), 7.91 (d, *J* = 8.4 Hz, 1H), 7.78 (s, 1H), 7.74 (t, *J* = 7.6 Hz, 1H), 7.65 (d, *J* = 8.3 Hz, 2H), 7.59–7.47 (m, 6H). ^{13}C{^{1}H} NMR (151 MHz, $CDCl_3$) δ (ppm): 155.8, 149.6, 149.0, 138.7, 138.4, 132.2, 130.3, 129.9, 129.7, 129.3, 128.8, 128.7, 126.8, 126.0, 125.9, 124.1, 119.0. HRMS (ESI+) m/z calcd $[M+H]^+$: 360.0387, found 360.0385.

***2-(4-Iodophenyl)-4-phenylquinoline*:**

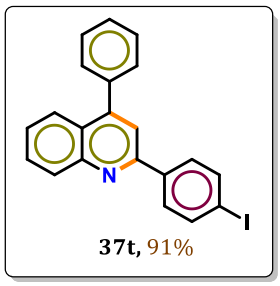

37t, 91%

^{1}H NMR (400 MHz, $CDCl_3$) δ (ppm): 8.22 (d, *J* = 8.4 Hz, 1H), 7.96 (d, *J* = 8.5 Hz, 2H), 7.90 (d, *J* = 8.3 Hz, 1H), 7.86 (d, *J* = 8.5 Hz, 2H), 7.78 (s, 1H), 7.76–7.72 (m, 1H), 7.57–7.47 (m, 6H). ^{13}C{^{1}H} NMR (101 MHz, $CDCl_3$) δ (ppm): 155.9, 149.6, 149.0, 139.3, 138.4, 138.1, 130.3, 129.9, 129.7, 129.4, 128.8, 128.7, 126.8, 126.1, 125.9, 119.0, 96.1. HRMS (ESI+) m/z calcd $[M+H]^+$: 408.0249, found 408.0251.

***2-(3,4-dimethoxyphenyl)-4-phenylquinoline*:**

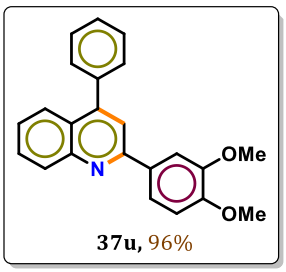

37u, 96%

^{1}H NMR (400 MHz, $CDCl_3$) δ (ppm): 8.23 (d, *J* = 8.2 Hz, 1H), 7.93–7.84 (m, 2H), 7.79 (s, 1H), 7.71 (ddd, *J* = 8.5, 5.3, 1.7 Hz, 2H), 7.60–7.49 (m, 5H), 7.45 (ddd, *J* = 8.2, 6.9, 1.2 Hz, 1H), 6.99 (d, *J* = 8.4 Hz, 1H), 4.06 (s, 3H), 3.96 (s, 3H). ^{13}C{^{1}H} NMR (101 MHz, $CDCl_3$) δ (ppm): 156.5, 150.6, 149.6, 149.2, 148.9, 138.7, 132.7, 130.0, 129.7, 129.6, 128.7, 128.5, 126.2, 125.8, 125.7, 120.4, 119.1, 111.2, 110.6, 56.2, 56.1. HRMS (ESI+) m/z calcd $[M+H]^+$: 342.1494, found 342.1488.

***2-methyl-7-phenyl-5,6-dihydrobenzo[c]acridine*:**

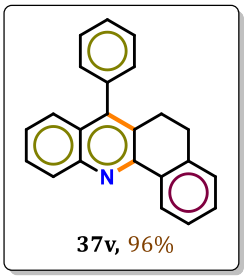

37v, 96%

^{1}H NMR (400 MHz, $CDCl_3$) δ (ppm): 8.65 (d, *J* = 7.7 Hz, 1H), 8.20 (d, *J* = 8.4 Hz, 1H), 7.65 (ddd, *J* = 8.4, 6.7, 1.6 Hz, 1H), 7.58–7.50 (m, 3H), 7.58–7.50 (m, 3H), 7.44 (dd, *J* = 10.7, 4.2 Hz, 2H), 7.41–7.36 (m, 2H), 7.35 – 7.31 (m, 2H), 7.28–7.23 (m, 1H), 2.91–2.84 (m, 4H). ^{13}C{^{1}H} NMR (101 MHz, $CDCl_3$) δ (ppm): 153.3, 147.4, 145.5, 139.5, 137.1, 135.3, 129.8, 129.7, 128.7, 128.6, 128.2, 128.1, 127.8, 127.5,

127.4, 126.5, 126.2, 126.1, 28.5, 26.7. HRMS (ESI+) m/z calcd $[M+H]^+$: 308.1439, found 308.1435.

4.6 Bibliography

[1] El Shehry, M. F., Ghorab, M. M., Abbas, S. Y., Fayed, E. A., Shedid, S. A., and Ammar, Y. A. Quinoline derivatives bearing pyrazole moiety: synthesis and biological evaluation as possible antibacterial and antifungal agents. *European Journal of Medicinal Chemistry*, 143:1463-1473, 2018.

[2] Matada, B. S., Pattanashettar, R., and Yernale, N. G. A comprehensive review on the biological interest of quinoline and its derivatives. *Bioorganic & Medicinal Chemistry*, 32:115973, 2021.

[3] Batista, V. F., Pinto, D. C., and Silva, A. M. Synthesis of quinolines: a green perspective. *ACS Sustainable Chemistry & Engineering*, 4(8):4064-4078, 2016.

[4] Weyesa, A. and Mulugeta, E. Recent advances in the synthesis of biologically and pharmaceutically active quinoline and its analogues: a review. *RSC Advances*, 10(35):20784-20793, 2020.

[5] Musiol, R. An overview of quinoline as a privileged scaffold in cancer drug discovery. *Expert Opinion on Drug Discovery*, 12(6):583-597, 2017.

[6] Kim, J. I., Shin, I. S., Kim, H. and Lee, J. K. Efficient electrogenerated chemiluminescence from cyclometalated iridium (III) complexes. *Journal of the American Chemical Society*, 127(6):1614-1615, 2005.

[7] Eswaran, S., Adhikari, A. V., Chowdhury, I. H., Pal, N. K., and Thomas, K. D. New quinoline derivatives: Synthesis and investigation of antibacterial and antituberculosis properties. *European Journal of Medicinal Chemistry*, 45(8):3374-3383, 2010.

[8] Chandrappa, M., Swathi, K., Kumar, S. G., and Pullela, P. K. Nanomaterial assisted bulk scale synthesis of 2-methyl-6-nitroquinoline. *Materials Today: Proceedings*, 37:1469-1474, 2021.

[9] Aivali, S., Tsimpouki, L., Anastasopoulos, C., and Kallitsis, J. K. Synthesis and optoelectronic characterization of perylene diimide-quinoline based small molecules. *Molecules*, 24(23):4406, 2019.

[10] Zhang, L., Wang, Y. F., Li, M., Gao, Q. Y., and Chen, C. F. Quinoline-based aggregation-induced delayed fluorescence materials for highly efficient non-

doped organic light-emitting diodes. *Chinese Chemical Letters*, 32(2):740-744, 2021.

[11] Friedlaender, P. Ueber o-Amidobenzaldehyd. *Berichte der deutschen chemischen Gesellschaft*, 15(2):2572-2575, 1982.

[12] Zheng, J., Li, Z., Huang, L., Wu, W., Li, J., and Jiang, H. Palladium-catalyzed intermolecular aerobic annulation of o-alkenylanilines and alkynes for quinoline synthesis. *Organic Letters*, 18(15):3514-3517, 2016.

[13] Sharma, R., Kour, P., and Kumar, A. A review on transition-metal mediated synthesis of quinolines. *Journal of Chemical Sciences*, 130:1-25, 2018.

[14] Chelucci, G. and Porcheddu, A. Synthesis of Quinolines *via* a metal-catalyzed dehydrogenative *N*-heterocyclization. *The Chemical Record*, 17(2):200-216, 2017.

[15] Chen, Z., Song, J., Peng, X., Xi, S., Liu, J., Zhou, W., Li, R., Ge, R., Liu, C., Xu, H., and Zhao, X. Iron single atom catalyzed quinoline synthesis. *Advanced Materials*, 33(34):2101382, 2021.

[16] Meyet, C. E. and Larsen, C. H. One-step catalytic synthesis of alkyl-substituted quinolines. *The Journal of Organic Chemistry*, 79(20):9835-9841, 2014.

[17] Das, S., Maiti, D., and De Sarkar, S. Synthesis of polysubstituted quinolines from α-2-aminoaryl alcohols *via* Nickel-catalyzed dehydrogenative coupling. *The Journal of Organic Chemistry*, 83(4):2309-2316, 2018.

[18] Khusnutdinov, R. I., Bayguzina, A. R., and Dzhemilev, U. M. Metal complex catalysis in the synthesis of quinolines. *Journal of Organometallic Chemistry*, 768:75-114, 2014.

[19] Yang, L. and Wan, J. P. Ethyl lactate-involved three-component dehydrogenative reactions: biomass feedstock in diversity-oriented quinoline synthesis. *Green Chemistry*, 22(10):3074-3078, 2020.

[20] Siddiki, S. H., Toyao, T., and Shimizu, K. I. Acceptorless dehydrogenative coupling reactions with alcohols over heterogeneous catalysts. *Green Chemistry*, 20(13):2933-2952, 2018.

[21] Wang, T. X., Liang, H. P., Anito, D. A., Ding, X., and Han, B. H. Emerging applications of porous organic polymers in visible-light photocatalysis. *Journal of Materials Chemistry A*, 8(15):7003-7034, 2020.

[22] Maji, M., Chakrabarti, K., Panja, D., and Kundu, S. Sustainable synthesis of *N*-heterocycles in water using alcohols following the double dehydrogenation strategy. *Journal of Catalysis*, 373:93-102, 2019.

[23] Das, K., Mondal, A., and Srimani, D. Phosphine free Mn-complex catalysed dehydrogenative C–C and C–heteroatom bond formation: a sustainable approach to synthesize Quinoxaline, Pyrazine, Benzothiazole and Quinoline derivatives. *Chemical Communications*, 54(75):10582-10585, 2018.

[24] You, B., Liu, X., Liu, X. and Sun, Y. Efficient H_2 evolution coupled with oxidative refining of alcohols *via* a hierarchically porous nickel bifunctional electrocatalyst. *ACS Catalysis*, 7(7):4564-4570, 2017.

[25] Xu, J. X., Pan, N. L., Chen, J. X., and Zhao, J. W. Visible-light-mediated oxidative cyclization of 2-Aminobenzyl alcohols and secondary alcohols enabled by an organic photocatalyst. *The Journal of Organic Chemistry*, 86(15):10747-10754, 2021.

[26] Pathak, D., Khatioda, R., Sharma, H., Guha, A. K., Saikia, L., and Sarma, B. Endorsing organic porous polymers in regioselective and unusual oxidative C═C bond cleavage of styrenes into aldehydes and anaerobic benzyl alcohol oxidation *via* hydride elimination. *ACS Applied Materials & Interfaces*, 13(13):15353-15365, 2021.

[27] Chan-Thaw, C. E., Villa, A., Prati, L., and Thomas, A. Triazine-based polymers as nanostructured supports for the liquid-phase oxidation of alcohols. *Chemistry–A European Journal*, 17(3):1052-1057, 2011.

[28] Du, C., Na, W., Shao, M., Shang, S., Liu, Y., and Chen, J. Self-templated synthesis of Triphenylene-based uniform hollow spherical two-dimensional covalent organic frameworks for drug delivery. *Chemistry of Materials*, 35(3):1395-1403, 2023.

[29] Feng, J. and Yin, Y. Self-templating approaches to hollow nanostructures. *Advanced Materials*, 31(38):1802349, 2019.

[30] Wei, D., Dorcet, V., Darcel, C., and Sortais, J. B. Synthesis of Quinolines through acceptorless dehydrogenative coupling catalyzed by Rhenium PN(H)P complexes. *ChemSusChem*, 12(13):3078-3082, 2019.

4.7 Representative Spectra

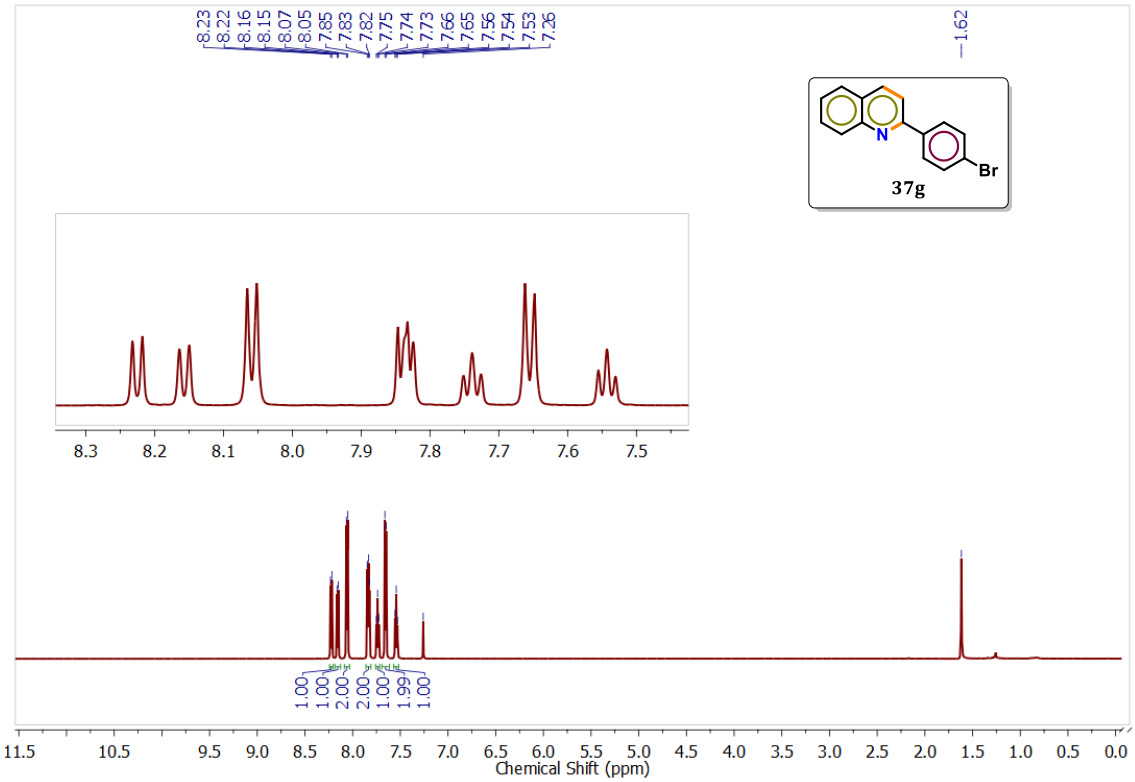

Figure 4.8 ^{1}H NMR ($CDCl_3$, 600 MHz, 298 K) of **37g**

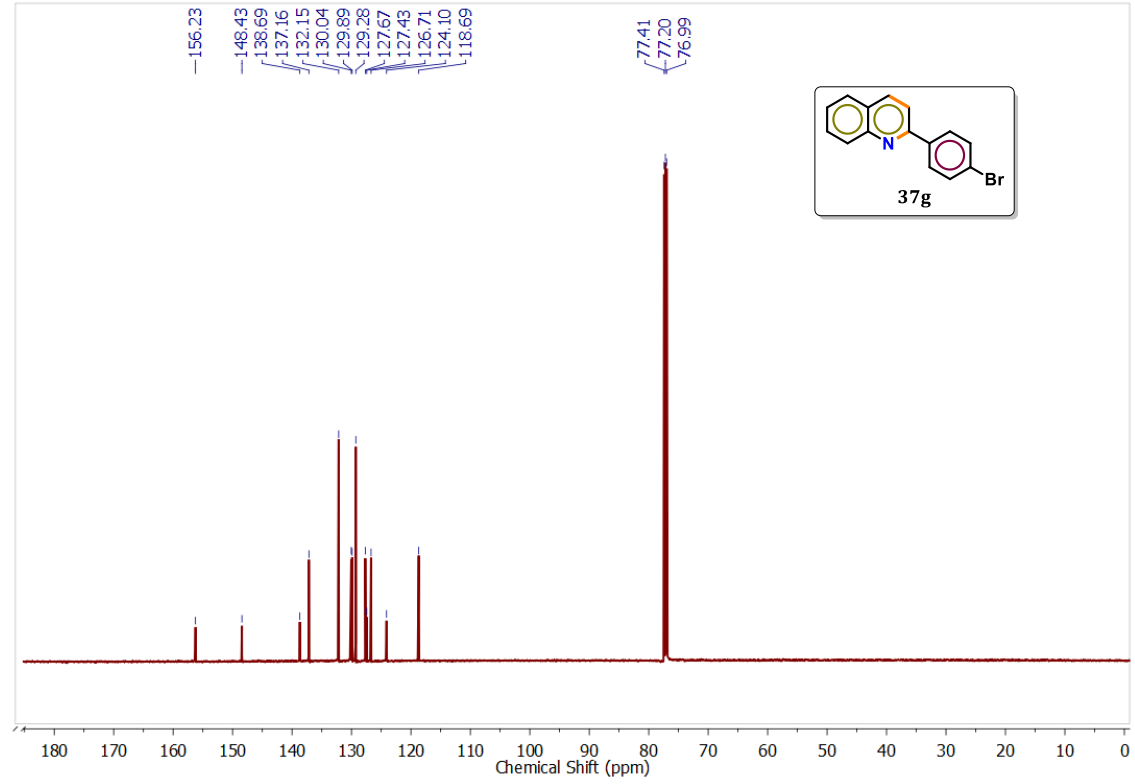

Figure 4.9 $^{13}C\{^{1}H\}$ NMR ($CDCl_3$, 151 MHz, 298 K) of **37g**

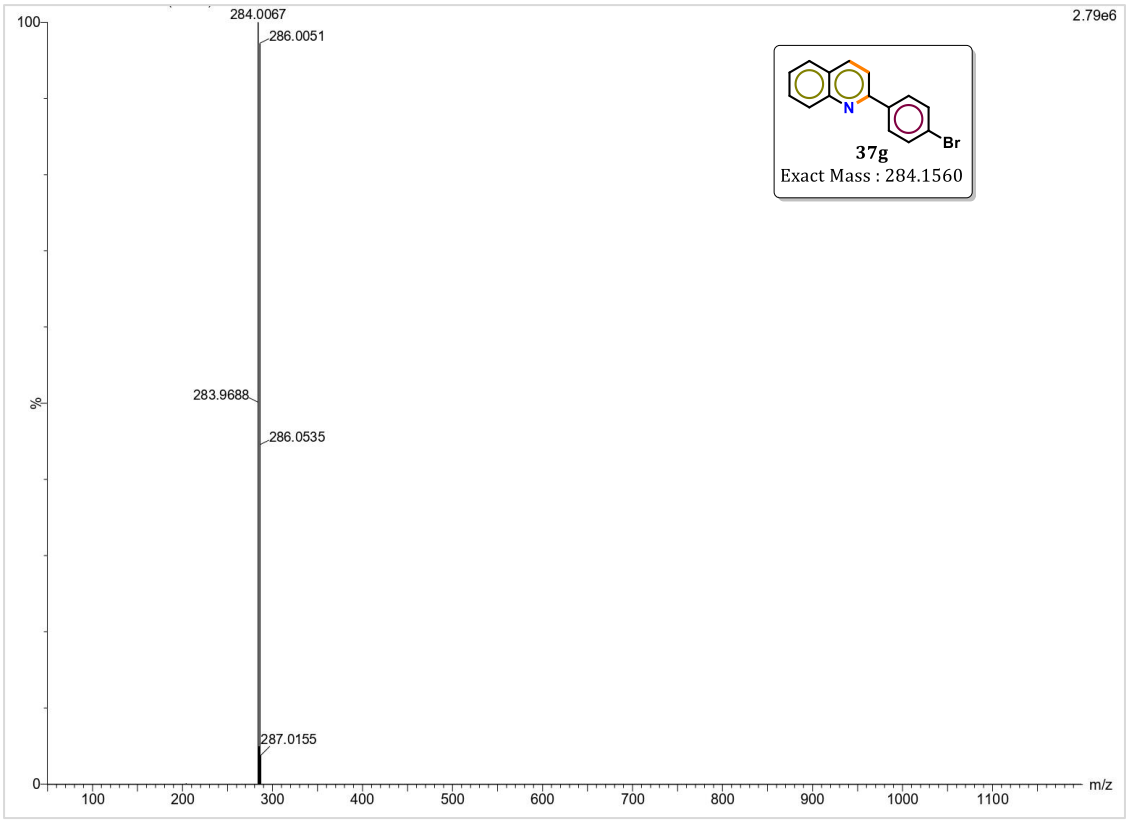

Figure 4.10 HRMS (ESI⁺) *m/z* of **37g**

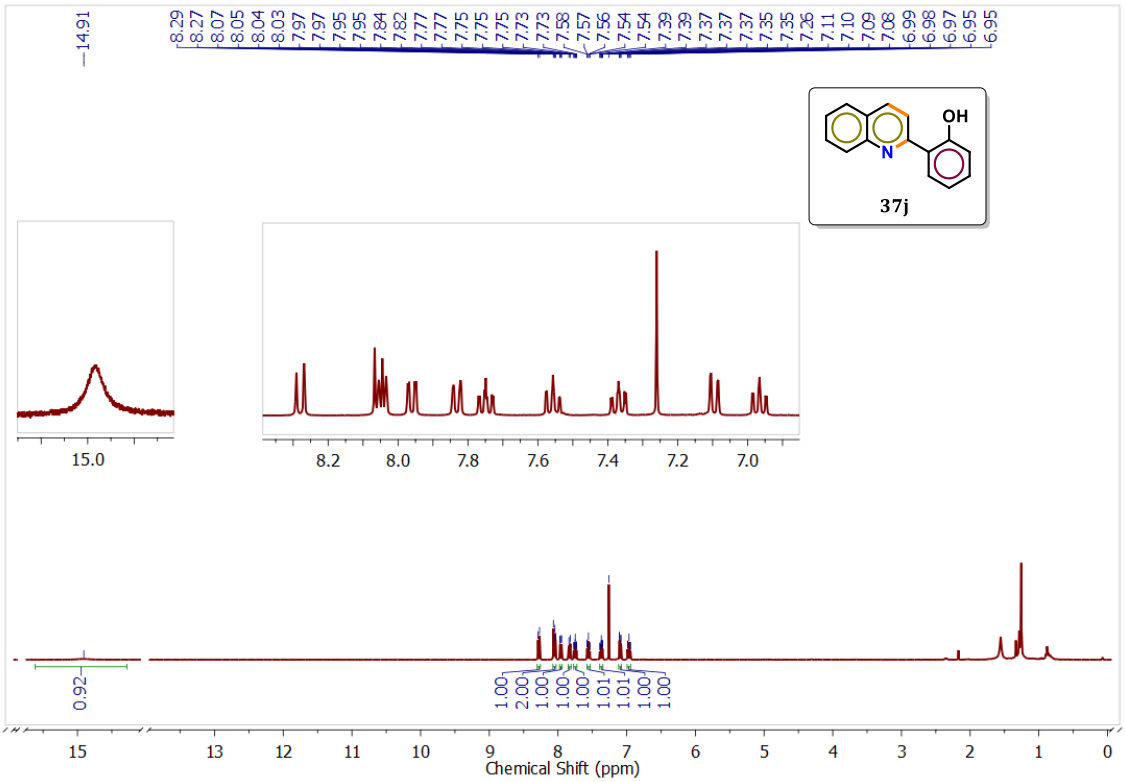

Figure 4.11 ^{1}H NMR ($CDCl_3$, 400 MHz, 298 K) of **37j**

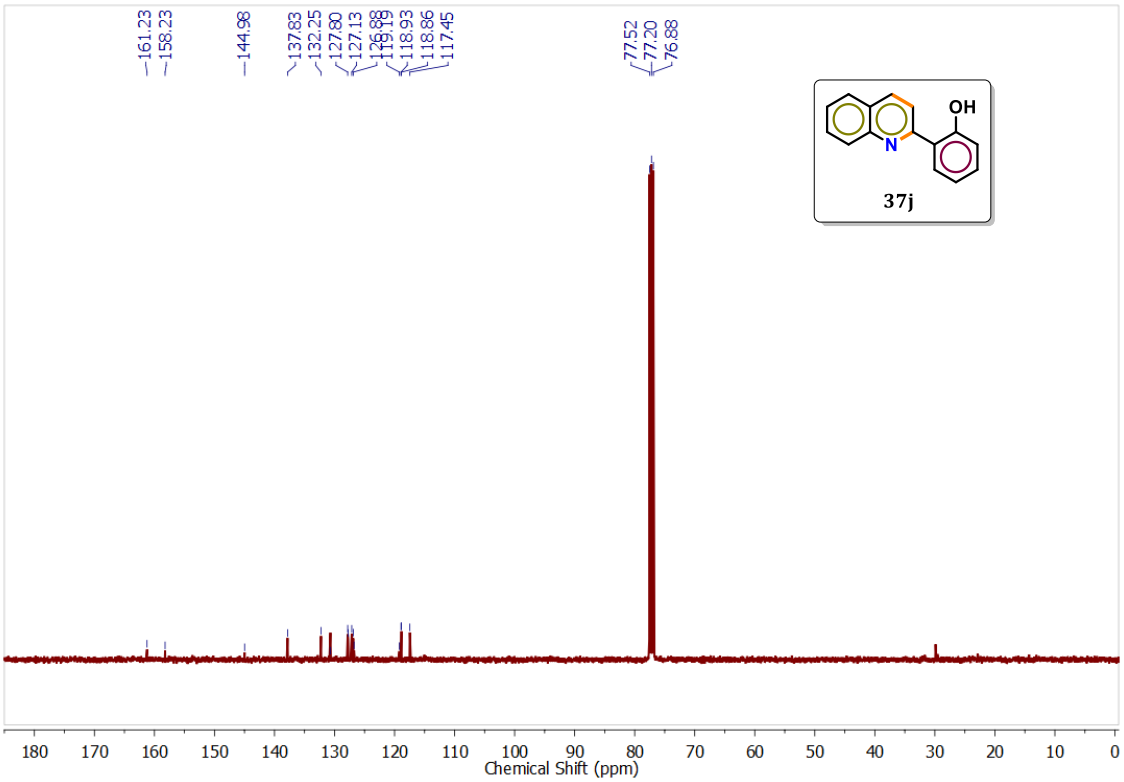

Figure 4.12 $^{13}C\{^{1}H\}$ NMR ($CDCl_3$, 101 MHz, 298 K) of **37j**

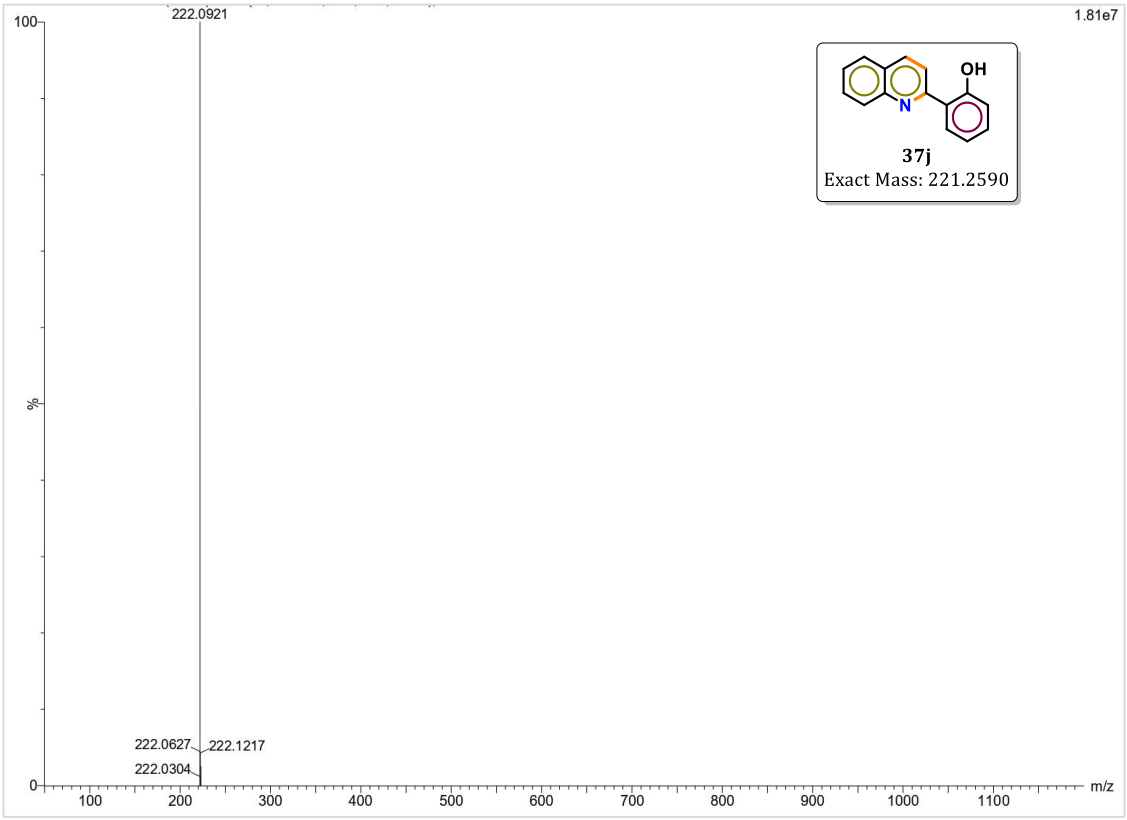

Figure 4.13 HRMS (ESI^+) *m/z* of **37j**

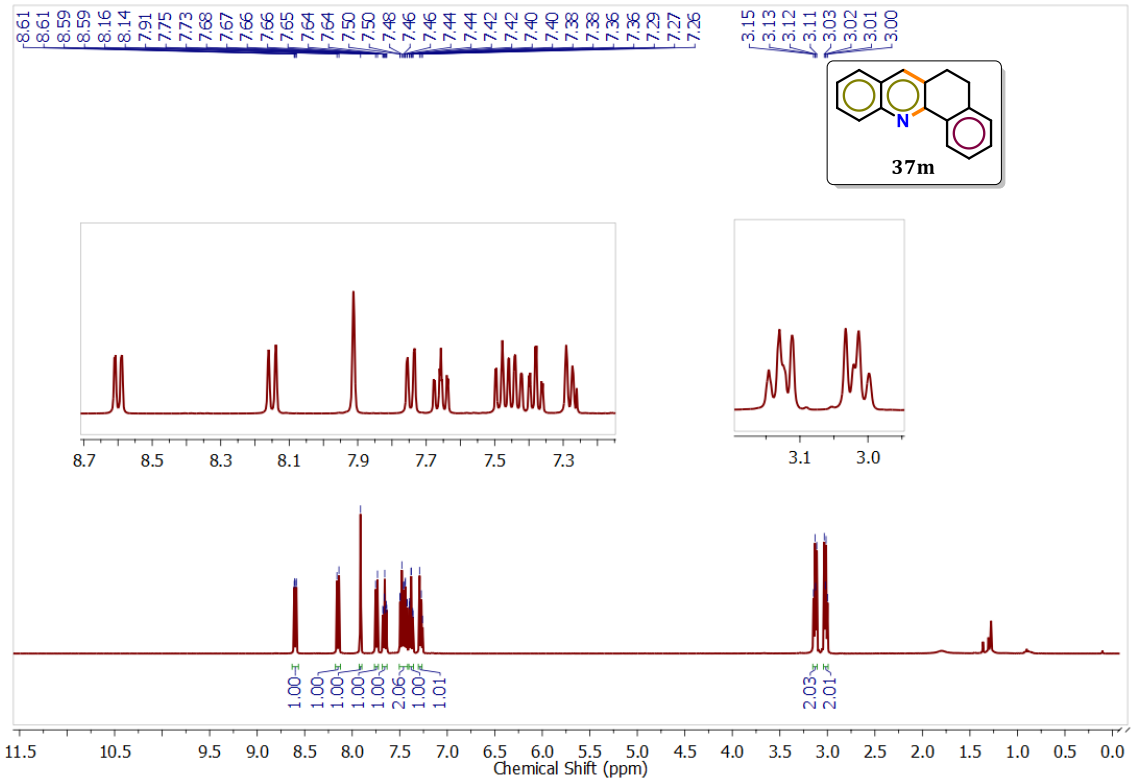

Figure 4.14 ^{1}H NMR ($CDCl_3$, 400 MHz, 298 K) of **37m**

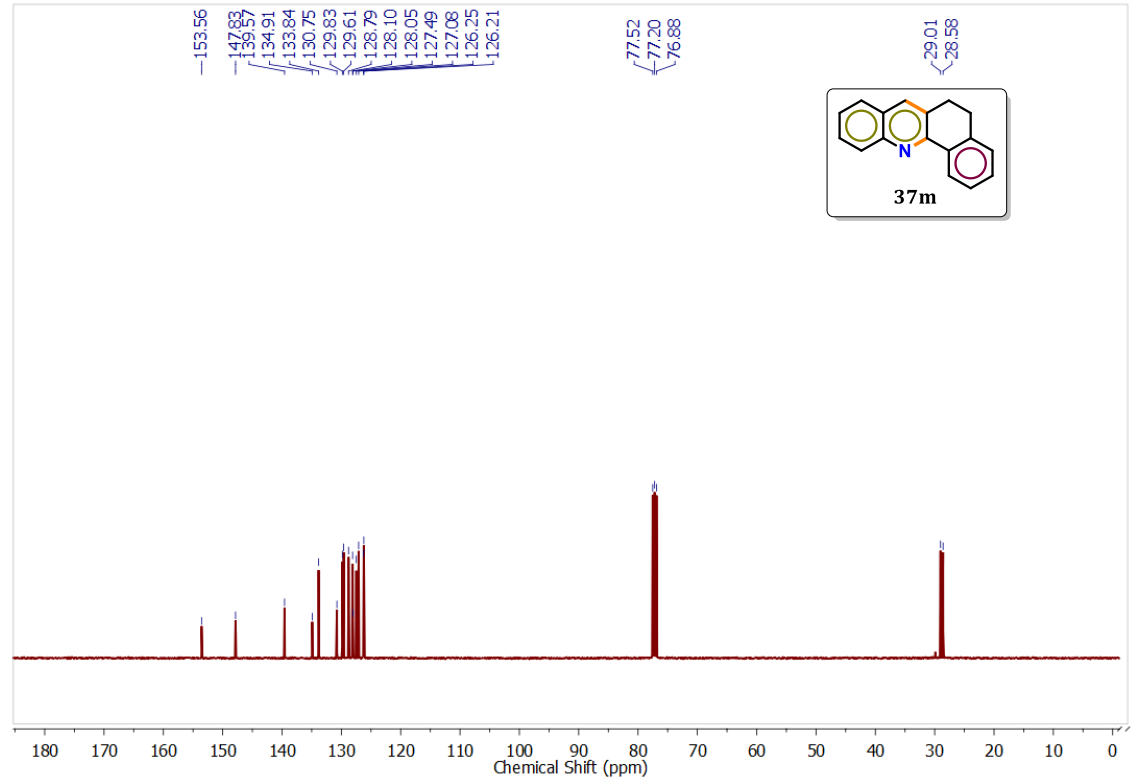

Figure 4.15 $^{13}C\{^{1}H\}$ NMR ($CDCl_3$, 101 MHz, 298 K) of **37m**

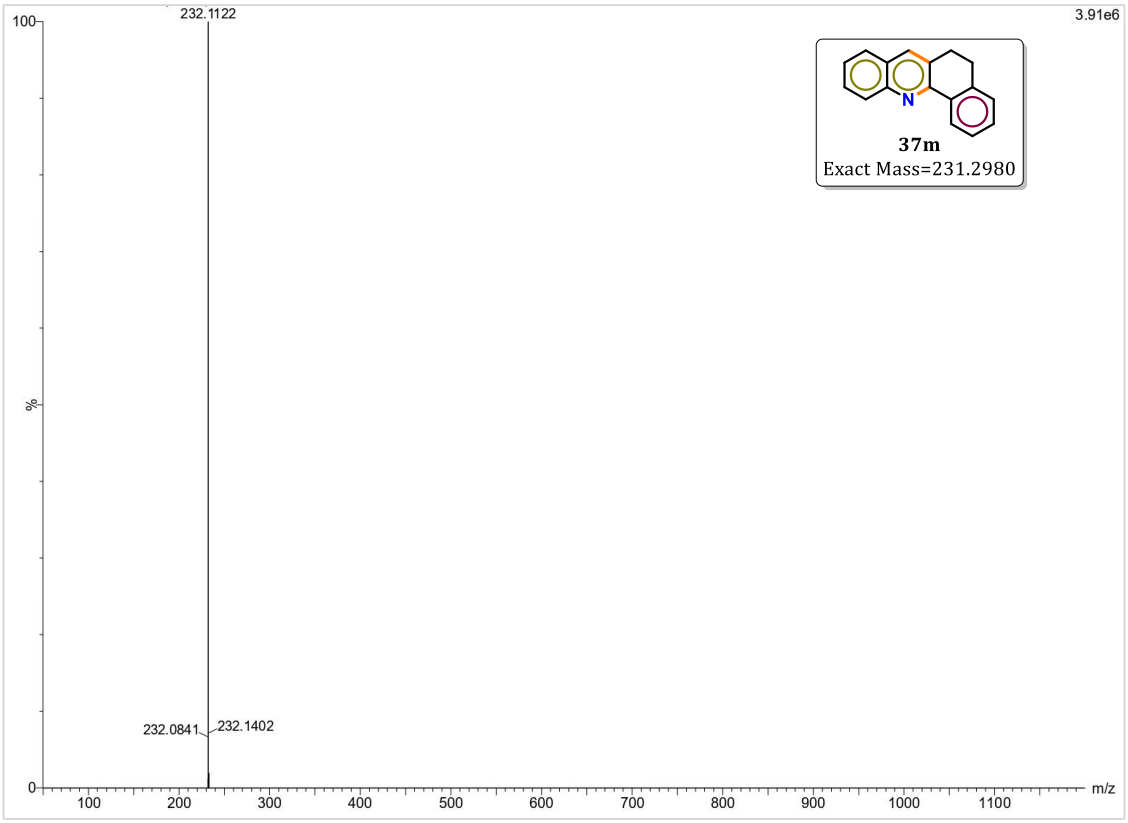

Figure 4.16 HRMS (ESI⁺) *m/z* of **37m**

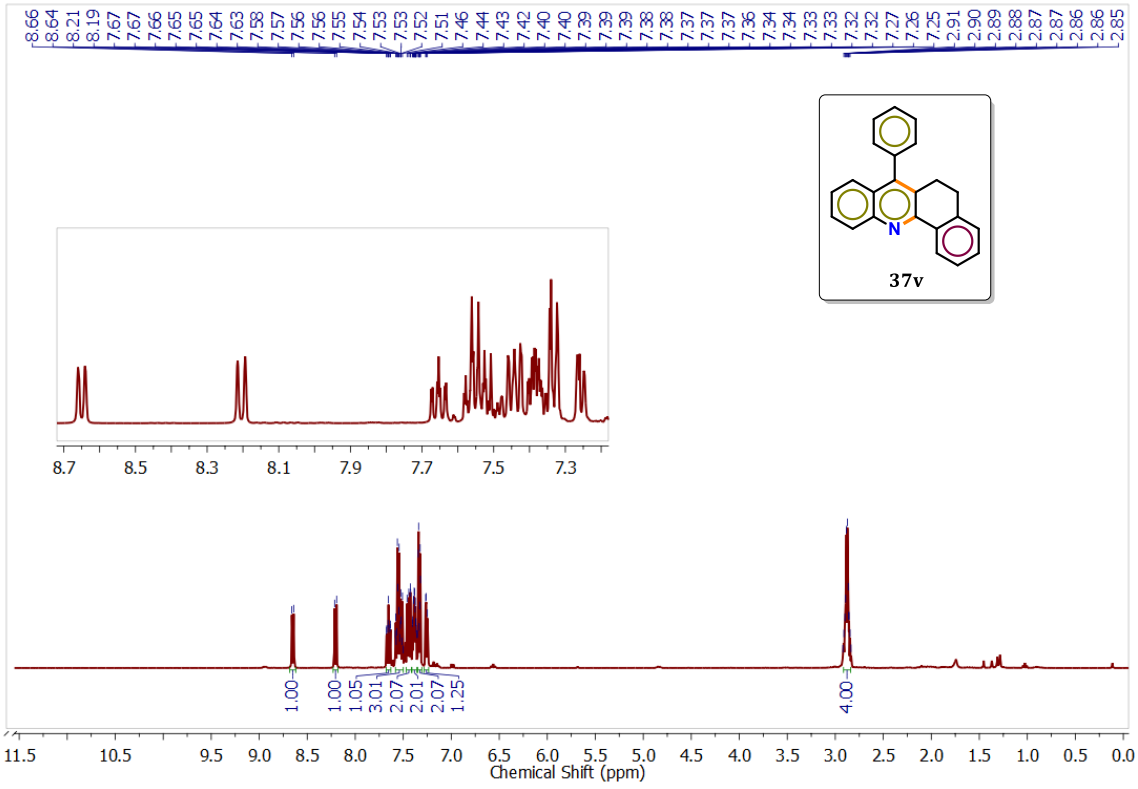

Figure 4.17 ^{1}H NMR ($CDCl_3$, 400 MHz, 298 K) of **37v**

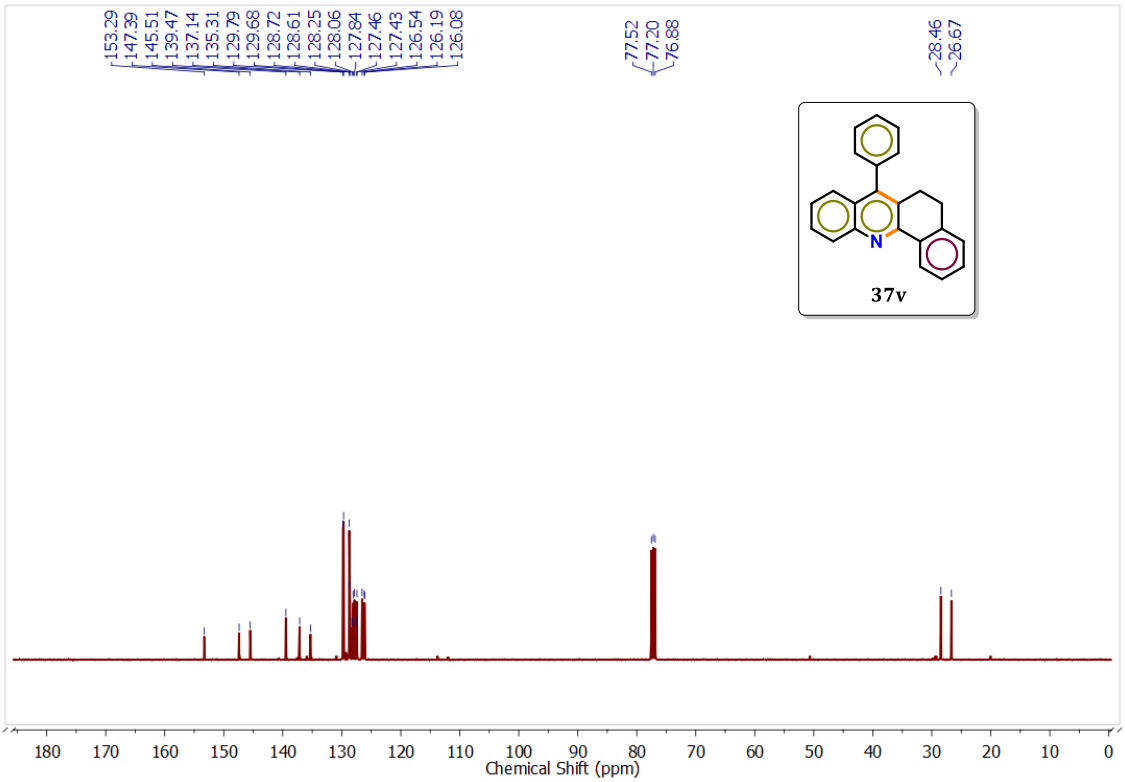

Figure 4.18 $^{13}C\{^{1}H\}$ NMR ($CDCl_3$, 101 MHz, 298 K) of **37v**.

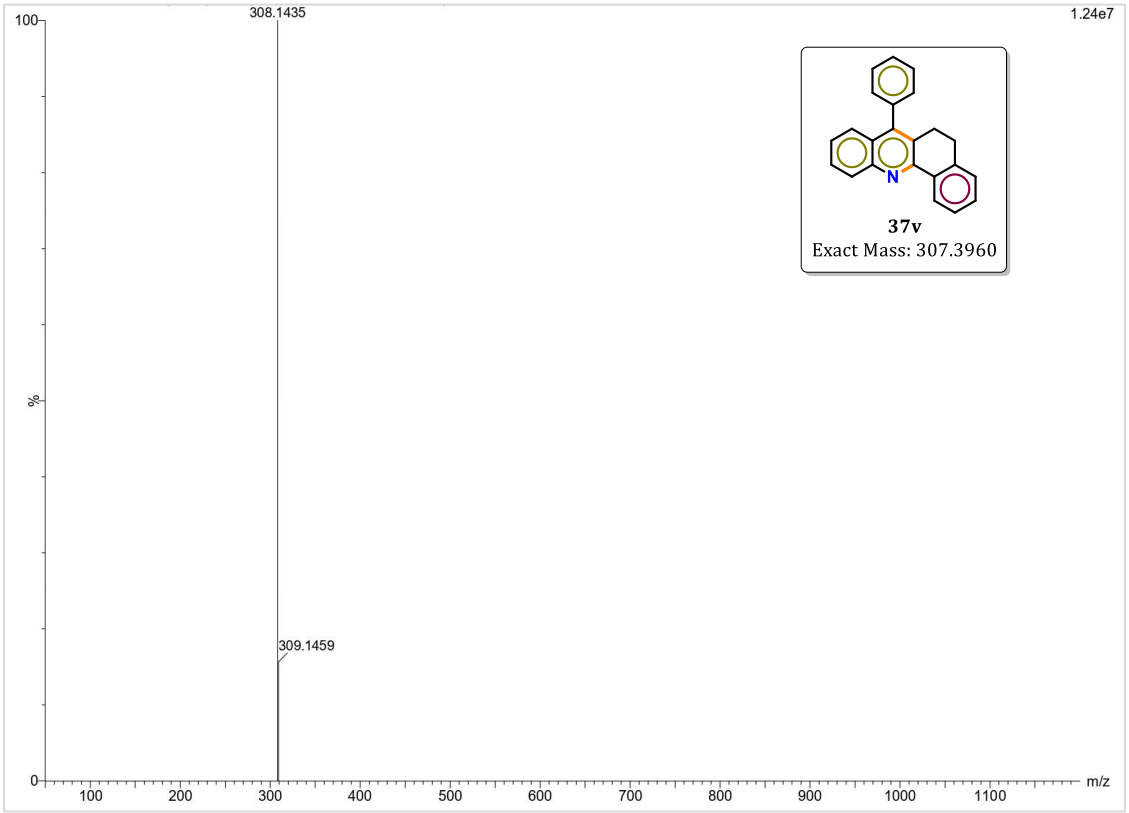

Figure 4.19 HRMS (ESI^+) *m/z* of **37v**